MA102 Mathematics
Fall 2020

Honz
Research
Institute of
Pharmacometrics and
Industrial
Engineering

Original Article

Access this article online
Website: www.ijtrichology.com
DOI: 10.4103/ijt.ijt_25_20
Quick Response Code:

Scalp hair whorl patterns in patients affected by Neurofibromatosis Type 1: A case-control study

Andrea Sechi, Iria Neri, Annalisa Patrizi, Michela Starace, Francesco Savoia, Miriam Leuzzi, Raffaele Dante Caposiena Caro[1], Bianca Maria Piraccini

Department of Experimental, Diagnostic and Specialty Medicine, Division of Dermatology, University of Bologna, Bologna, [1]Department of Systems Medicine, Dermatology Unit, University of Rome Tor Vergata, Rome, Italy

Address for correspondence: Prof. Annalisa Patrizi, Department of Experimental, Diagnostic and Specialty Medicine, Division of Dermatology, University of Bologna, Via Massarenti, 1, 40138 Bologna, Italy. E-mail: annalisa.patrizi@unibo.it

Submitted: 21-Feb-2020
Revised: 14-Mar-2020
Accepted: 21-Mar-2020
Published: 05-May-2020

ABSTRACT

Background: The hair whorl denotes the spiral disposition of hairs around an axis, which is determined by the follicle growing direction. Atypical variants of scalp hair patterns, identified by abnormally placed or multiple whorls, have been associated with early brain developmental disorders and several dysmorphic syndromes. **Materials and Methods:** A 6-month case–control, prospective monocentric study included an overall number of 557 children. A logistic regression analysis was performed to evaluate the relationship between localization, the number of scalp hair whorls, and their association with neurofibromatosis type 1 (NF1). **Results:** NF1 positively correlates with a frontal localization, whereas a negative association was found with a parietal whorl pattern ($P < 0.001$). **Conclusion:** Evaluation of scalp whorls gains importance in the neonatal settings and may contribute to suspect the early diagnosis of NF1, as the related National Institutes of Health diagnostic criteria cannot be usually observed at an early age.

Key words: Hair whorls, neurofibromatosis type 1, scalp pattern

INTRODUCTION

The term "hair whorl" describes the circular distribution of hairs on the scalp that revolves around an axis, which is determined by the follicle growing direction.[1] Hair whorl patterns are characterized by the orientation or spin, the overall whorl number within the scalp, and the anatomical localization [Figure 1]. Among the many hypotheses done on their origin, most speculated the association between the hair whorls and central nervous system abnormalities.[2-4] Familiar clusters have been reported in the literature, and a possible genetic linkage has been postulated.[5]

The majority of the Caucasian population has a single apical scalp whorl, located in the parietal region underlying the vertex, either to the right of midline (56%), to the left (30%), or midline (14%).[6] The clockwise orientation is detected in 84% of the cases, while only 16% of hair whorls rotate counterclockwise.[7] Hair whorls' features are still evaluated using the Ziering Classification.[1] In 2003, Furdon and Clark analyzed scalp whorl features distinguishing between Afro-Americans and Caucasians.[8] This distinction was necessary because a single apical whorl is detected in 95.5% of Caucasians, but only in 10% of African Americans, who present a double apical hair whorl in 90% of the cases.[9]

An anterior hair whorl, either clockwise or counterclockwise, is commonly found in trisomy 21 and Prader–Willi

How to cite this article: Sechi A, Neri I, Patrizi A, Starace M, Savoia F, Leuzzi M, *et al*. Scalp hair whorl patterns in patients affected by neurofibromatosis type 1: A case-control study. Int J Trichol 2020;12:56-61.

syndrome, while its association with microcephaly, Rubinstein–Taybi syndrome, and X-linked mental retardation remains anecdotal, being reported only in a few cases [Figure 2].[6,10-13] The coexistence of two or more hair whorls has been associated with mental retardation,[4] developmental and neurological disorders such as autism,[14] and epilepsy,[15] and it correlates with defects of cranial bones, including dicephaly and trigonocephaly [Figure 3].[6] Moreover, multiple hair whorls have been associated with facial dysmorphisms and inflammatory dermatological diseases such as guttate psoriasis.[16,17]

On the other hand, the lack of hair whorls had been related to microcephaly and encephalocele[10,16] even though it can occur in healthy individuals.[6]

In the clinical practice, hair whorls are often overlooked. Examining the hair whorl pattern, physicians should pay attention when a hair whorl pattern is not localized on the parietal region or when multiple whorls are present on the scalp. Based on the previous observations, atypical localization or an increased number in hair whorls does not necessarily imply any disease, since in healthy individuals, hair whorls with atypical localizations, spins, or numbers may be observed.[17]

The purpose of this study is to assess any possible association between hair whorl patterns and neurofibromatosis type 1 (NF1) in pediatric patients who have attended the dermatology clinic of Bologna University (Italy) during a period of 6 months.

MATERIALS AND METHODS

In a prospective monocentric observation study performed from September 2019 to the end of January 2020, we registered the number, spin, and location of hair whorls in children affected by NF1 (according to the diagnostic criteria as reported in the National Institutes of Health consensus development conference)[18] versus control pediatric patients affected by acute transitory skin conditions, and referred to the Emergency Unit of Pediatric Dermatology, at the Sant'Orsola-Malpighi University Hospital of Bologna during the same period. None of the controls had a genetic syndrome or inherited skin disease.

All patients were included after the parents had signed informed consent. In all patients, a detailed analysis of the scalp was performed. The hair whorl pattern was obtained by a different combination of three variable factors: whorl number, localization (parietal, frontal, and occipital area), and orientation (clockwise or counterclockwise).

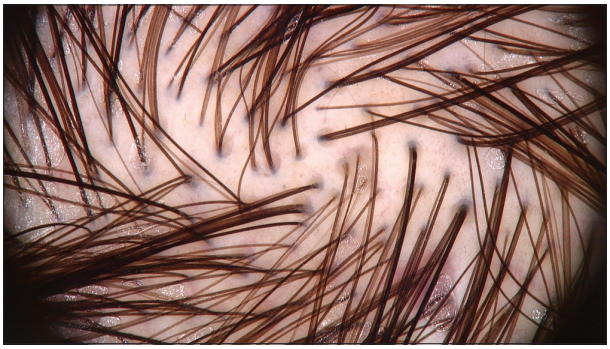

Figure 1: Trichoscopy of a scalp hair whorl: The hairs emerging from the scalp form a clockwise S-shaped spiral due to their oblique orientation

Figure 2: Frontal clockwise hair whorl in a patient affected by neurofibromatosis type 1

Figure 3: Double clockwise parietal whorls in a control

An exclusion criterion was the impossibility to perform a correct assessment of the scalp hair pattern. Diseases characterized either by cicatricial or reversible hair loss, the presence of alopecia areata, or nonpathological

conditions such as the use of grooming techniques in patients with crinkled or very long hairs contraindicated patient recruitment.

The primary endpoint was to assess the frequency of scalp hair patterns in affected patients versus controls in the studied population. The second endpoint was to examine the possible association between a target whorl pattern and NF1.

For any hair whorl pattern, a statistical correlation of their frequencies among affected versus nonaffected participants, expressed as dichotomous variables, was analyzed by a binomial logistic regression. Proportions were estimated with 95% exact confidence interval, and statistical significance was assessed at $P < 5\%$ (0.05). All analyses were performed using IBM® SPSS® Statistics for Windows Version 23.0 (IBM Corp., Armonk, NY, USA). All examinations were performed in accordance with the Helsinki principles of medical ethics.

RESULTS

An overall number of 501 pediatric patients, all Caucasians, were included in the study and served as controls (median age: 11.22 years; standard deviation [SD]: 6.32, female/male ratio: 1.13). Controls' hair whorl patterns are reported in Table 1.

The reported clinical conditions were, in order of decreasing frequency: infective skin disorders (234/501, 46.7%), exogenous dermatitis (108/501, 21.6%), cutaneous burns (47/501, 9.4%), paraviral or postinfectious skin eruptions (43/501, 8.6%), urticaria and/or angioedema (38/501, 7.6%), exanthematous diseases (25/501, 5%), and adverse drug reactions (6/501, 1.2%).

Patients affected by NF1 were 56 (median age: 13.9; SD: 5.4, female/male ratio: 1.56). Positive family history for NF1 was reported in 37/56 cases. Hair whorl patterns in patients affected by NF1 are shown in Table 1.

The great majority of the controls showed a single hair whorl localized in the vertex area, with the hair oriented in a clockwise direction (352/501: 70.3%), while only 15.7% (76/501) of the patients had a single counterclockwise vertex whorl. Two scalp whorls were detected in 12.4% of the cases, with the parietal areas again been the most common localization. 66.1% of whorl duplets were co-localized within the same areas. The duplet spins were oriented both clockwise in 8 whorl pairs (19%), both counterclockwise in 2 cases (4.8%), or combined in a counterclockwise/clockwise pattern in the remaining 71.4% of the cases. A triple scalp whorl was very infrequent, being detected only in 9 patients. In none of these cases, the triplets were co-localized within the same areas and combined very heterogeneously.

The statistical analysis [Table 2] showed a positive correlation between the frontal hair whorl localization and NF1 was found ($P < 0.001$), whereas an inverse association between parietal location and NF1 was detected ($P < 0001$).

Table 1: Scalp hair whorl patterns in neurofibromatosis type 1 and controls

Hair whorls per patient	Number of patients	Hair whorl number, localization, and spin									Total whorl number
		Parietal			Frontal			Occipital			
		CW	CCW	Both	CW	CCW	Both	CW	CCW	Both	
Controls											
Zero	2	-	-	-	-	-	-	-	-	-	0
One	428	352	76	-	-	-	-	-	-	-	428
Two	62	76 (8)	25 (2)	- (30)	5		-	12	6	- (1)	124
Three	9	13 (3)	6	- (3)	1	-	-	4	3	- (2)	27
Total	501	441 (11)	107 (2)	- (33)	6	0	0	16	9	- (3)	579
NF1 patients											
Zero	-	-	-	-	-	-	-	-	-	-	
One	47	38	-	-	9	-	-	-	-	-	47
Two	8	9 (1)	2	- (1)	2	1	-	2	-	-	16
Three	1	1	1	- (1)	1	-	-	-	-	-	3
Total	56	48 (1)	3	(2)	12	1	-	-	2	-	66

Both cases and controls showed a single hair whorl (83.9% and 85.4%, respectively). Two scalp whorls were detected in 14.3% of the cases and in 12.4% of the controls, while a triple scalp whorl was very infrequent. The prevalence of frontal whorls was 1% and 19.7% in controls and NF1 patients, respectively. The mismatch between the number of patients and the total number of scalp whorls is due to the count of every single element in cases of multiple whorls. Double parentheses denote the features of whorl duplets that are co-localized on the scalp area of the same patient. None of the triplets are co-localized within the same scalp area in patients presenting with 3 hair whorls. NF1 – Neurofibromatosis type 1; CW – Clockwise; CCW – Counterclockwise

Table 2: Linear and logistic regression

Factor	Coefficient	CI	*P*
Absent whorls	−19.016	0	0.999
Single whorls	−0.116	0.14-1.895	0.764
Double whorls	0.166	0.533-2.611	0.683
Triple whorls	−0.006	0.124-7.993	0.995
Frontal area	**3.114**	**8.054-62.857**	**<0.001***
Parietal area	**−3.459**	**0.008-0.120**	**<0.001***
Occipital area	−0.215	0.185-3.523	0.775

Significant features are set in bold. *Significant (P<0.05). CI – Confidence interval

DISCUSSION

The study of hair patterning has a long history. The reasons for clinicians' interest in hair whorls vary considerably. First and foremost, the scalp hair pattern remains unchanged from birth until death and is an easy and identifiable sign.

Multiple nonmutual exclusive theories concerning the determinants of the hair directional pattern have been postulated. The oldest yet still the most validated remains the mechanical theory, which states that the domelike growth of the underlying brain affects the hair directional slope.[11] The key factor is played by the plane of stretch exerted on the skin by underlying growing tissue during the hair follicle development in fetal life.[6] Therefore, all disorders of early brain development (including encephalocele, cervical neural groove, dicephaly, and microcephaly) occurring within the first 18 weeks of fetal life are critical for the establishment of the hair follicle formation within the scalp and result in an aberrant scalp hair patterning.[18] Hair follicles precursors, derived from the neuroectoderm, penetrate into the underlying mesenchyme with a sloping angle due to the relative increase of growing tension on the epidermis compared to the underlying layers. The angle of inclination formed by the emerging hair follicle with the skin is highly conserved in groups of nearby hair follicles, thus creating a hair tract. A hair stream is determined when two or more hair tracts take a different direction: as a consequence, from a tight apical whorl, the parietal hair stream progresses centrifugally to cover the whole scalp.[6,10]

A recent advance in the understanding the formation of scalp whorls has been made by Paul, who were able to generate high dermoepidermal shearing forces on pigskin using tissue expanders. As a consequence, the resulting rapid tissue expansion induces the formation of spirals along the advancing line of cellular proliferation, which progressively deformed into curves, to finally generate the whorl pattern.[19]

A genetic factor conditioning scalp whorl patterning has been put forward in order to explain hair whorl formation in scalp areas lacking mechanical tension forces during embryogenesis.[17] This theory has been validated by investigations based on the study of left-handedness, counterclockwise scalp whorls, and atypical right hemisphere location of the language center.[20]

Moreover, a metabolic etiology has been proposed. This theory supports the observation that hair follicles tend to be evenly spaced, suggesting that the activity of promoting and inhibiting growth factors conditions the distribution of the follicular units within the scalp. The hair whorl becomes the center of a decreased metabolic activity, due to the reduced release of morphogens.[21]

Recent studies on mammals with hair whorls in the coat showed that the variation may arise from sequence variation in the genes involved in tissue polarity signaling, including Frizzled 6, a member of a large family of integral membrane Wnt receptors.[22] The same system that patterns hair may also play a role in regulating the development of genetic brain anomalies.[22]

Moore *et al*. studied the growth of the first hair coat in male mice administered with epidermal growth factor (EGF). The authors demonstrated that EGF plays a part in hair follicle development, and administering EGF in male mice caused hair whorl formation, resulting from the focal development of curved monotrichs, characterized by reduced diameter and length.[23] This finding becomes fascinating if tied to the ongoing debate concerning the EGF-receptor (EGF-R) role in Schwann cell tumor genesis, which is characteristic of NF1.[24] An EGF-overexpressing genotype was associated with the early onset of NF1 clinical features.[25] In addition, the EGF immunoreactivity was detected in week 15–16 fetuses at the level of surface epithelia.[26] On the skin, the highest staining intensity was localized at the follicular ostia. The outer root sheath, and the Henle layer of inner root sheath above the papilla, showed both a positive immunoreaction.[26] It is not clear how the EGF signaling pattern may condition the genesis of an abnormal whorl pattern; on the other hand, it is certain that this process is accomplished early, during the embryonic life.

By combining the different hypotheses upon the hair whorl formation, it is possible that the overexpression of EGF-R, already proved in NF1 murine tumor models,[27] changes according to the different scalp areas. The EGF-driven metabolic response could trigger growth signals within the follicular units, altering their distribution and orientation

in the scalp. However, the involvement of a mechanical component in the pathogenesis cannot be excluded.

The results of this study show that atypical frontal scalp hair whorls can be a premonitory sign of NF1, even though they can also be rarely detected in normal controls.

No significant association was found between double scalp whorls and NF1. The data in our series show a prevalence of double scalp whorls, the majority co-located in the parietal area, with 12.37% in controls and 14.28% in NF1 affected patients. The prevalence found in the control group is quite surprising since it is double that reported in the literature, which stands at 4.5%.[11]

The collected results showed a 1% (6/579) and 19.7% (12/66) prevalence of frontal hair whorls in controls and NF1 patients, respectively.

A previous study on 510 pediatric patients referred for dermatological consultations reported an overall prevalence of frontal whorls in 7.8%, which peaked at 17.14% in the subcohort affected by inherited skin disorders, without providing the accounted diseases.[7]

Smith and Gong characterized scalp whorl features in 200 Caucasian children, describing a 10% moderate out flare of the medial eyebrow patterning, and the anterior scalp hair upsweep in 7% of the patients, which does not imply the formation of a frontal hair whorl.[11] Anterior frontal whorls were reported to be associated with the cowlick pattern in 7% of the cases, which are located along the frontal hairline.[6]

CONCLUSION

In the literature, there is little evidence regarding aberrant scalp hair directional patterning in patients affected by NF1. Frontal hair whorl localization has been associated with NF1, but a focused case–control study is still lacking.[7,28-30] Evaluation of scalp whorls gains importance in the neonatal setting, as the National Institutes of Health diagnostic criteria for NF1 cannot usually be observed at an early age but develop later in life.[18]

Financial support and sponsorship

Nil.

Conflicts of interests

There are no conflicts of interest.

REFERENCES

1. Ziering C, Krenitsky G. The Ziering whorl classification of scalp hair. Dermatol Surg 2003;29:817-21.
2. Samlaska CP, Benson PM, James WD. The ridgeback anomaly. A new follicular pattern of the scalp. Arch Dermatol 1989;125:98-102.
3. Yousefi-Nooraie R, Mortaz-Hedjri S. Dermatoglyphic asymmetry and hair whorl patterns in schizophrenic and bipolar patients. Psychiatry Res 2008;157:247-50.
4. Tirosh E, Jaffe M, Dar H. The clinical significance of multiple hair whorls and their association with unusual dermatoglyphics and dysmorphic features in mentally retarded Israeli children. Eur J Pediatr 1987;146:568-70.
5. Brewster ET. The inheritance of 'double crown'. J Hered 1925;16:345-6.
6. Smith DW, Gong BT. Scalp-hair patterning: Its origin and significance relative to early brain and upper facial development. Teratology 1974;9:17-34.
7. Milano A, De Palma M. Scalp hair whorl. Epidemiological study in 510 subjects. Eur J Pediatr Dermatol 2013;23160-7.
8. Furdon SA, Clark DA. Scalp hair characteristics in the new-born infant. Adv Neonatal Care 2003;3:286-96.
9. Wunderlich RC, Heerema NA. Hair crown patterns of human newborns. Studies on parietal hair whorl locations and their directions. Clin Pediatr (Phila) 1975;14:1045-9.
10. Kiil V. Frontal hair direction in mentally deficient individuals with special reference to mongolism. J Hered 1948;39:281-5.
11. Smith DW, Gong BT. Scalp hair patterning as a clue to early fetal brain development. J Pediatr 1973;83:374-80.
12. Hall BD, Smith DW. Prader-Willi syndrome. A resumé of 32 cases including an instance of affected first cousins, one of whom is of normal stature and intelligence. J Pediatr 1972;81:286-93.
13. Samlaska CP, James WD, Sperling LC. Scalp whorls. J Am Acad Dermatol 1989;21:553-6.
14. Aksu F, Baykara B, Ergın C, Arman C. Phenotypic features in autistic individuals: The finger length ratio (2D:4D), hair whorl, and hand dominance. Turk Psikiyatri Derg 2013;24:94-100.
15. Csabi G, Zsuppán R, Jeges S, Tényi T. Minor physical anomalies are more common in children with idiopathic epilepsy. Neuropsychopharmacol Hung 2014;16:115-20.
16. Ruiz-Maldonado R. A previously unreported syndrome of multiple scalp whorls and associated anomalies. Clin Exp Dermatol 2002;27:21-3.
17. Malathi M, Chandrasekhar L, Thappa DM. Multiple hair whorls in a child with normal cranial and neurologic development. Pediatr Dermatol 2013;30:630-1.
18. National Institutes of Health Consensus Development Conference Statement: Neurofibromatosis. Bethesda, Md., USA, July 13-15, 1987. Neurofibromatosis 1988;1:172-8.
19. Paul SP. Golden spirals and scalp whorls: Nature's own design for rapid expansion. PLoS One 2016;11:e0162026.
20. Jansen A, Lohmann H, Scharfe S, Sehlmeyer C, Deppe M, Knecht S. The association between scalp hair-whorl direction, handedness and hemispheric language dominance: Is there a common genetic basis of lateralization? Neuroimage 2007;35:853-61.
21. Mooney JR, Nagorcka BN. Spatial patterns produced by a reaction-diffusion system in primary hair follicles. J Theor Biol 1985;115:299-317.
22. Guo N, Hawkins C, Nathans J. Frizzled6 controls hair patterning in mice. Proc Natl Acad Sci U S A 2004;101:9277-81.
23. Moore GP, Panaretto BA, Robertson D. Effects of epidermal growth factor on hair growth in the mouse. J Endocrinol 1981;88:293-9.
24. DeClue JE, Heffelfinger S, Benvenuto G, Ling B, Li S, Rui W, *et al*. Epidermal growth factor receptor expression in neurofibromatosis type 1-related tumors and NF1 animal models. J Clin Invest 2000;105:1233-41.
25. Ribeiro R, Soares A, Pinto D, Catarino R, Lopes C, Medeiros R. EGF genetic polymorphism is associated with clinical features but not malignant phenotype in neurofibromatosis type 1 patients. J Neurooncol 2007;81:225-9.

26. Poulsen SS, Kryger-Baggesen N, Nexø E. Immunohistochemical localization of epidermal growth factor in the second-trimester human fetus. Histochem Cell Biol 1996;105:111-7.
27. Li H, Velasco-Miguel S, Vass WC, Parada LF, DeClue JE. Epidermal growth factor receptor signaling pathways are associated with tumorigenesis in the Nf1:p53 mouse tumor model. Cancer Res 2002;62:4507-13.
28. Pivnick EK, Lobe TE, Fitch SJ, Riccardi VM. Hair whorl as an indicator of a mediastinal plexiform neurofibroma. Pediatr Dermatol 1997;14:196-8.
29. Bonifazi E, Annicchiarico G. Vortice di capelli frontale. Eur J Pediat Dermatol 2005;15:185.
30. Milano A. Frontal whorl. An early sign of peripheral neurofibromatosis? Eur J Pediat Dermatol 2013;23:113.

The Secret of Hair Whorl

A View from Algebraic Topology

Nanfang Hong

February 7, 2021

Contents

Chapter 1

Basic Surface Algebraic Topology

This lecture is about surface algebraic topology. The key idea is to build a bridge between topology, which is abstract and hard to imagine, and algebraic structure, which is tangible and can be computed. In a categorical sense, we construct a functor

$$\mathfrak{C}_1 \to \mathfrak{C}_2$$

between two categories[1] with structural information preserved, namely

$$\mathfrak{C}_1 = \{\text{Topological Spaces, Homeomorphisms}\}$$
$$\mathfrak{C}_2 = \{\text{Groups, Homomorphisms}\}$$

Definition 1 (Topological Type)**.** All oriented compact surfaces can be classified by their genus g and number of boundaries b. Therefore, we use

$$(g, b)$$

to represent the topological type of an oriented surface $\mathbf{S}$.

Definition 2 (Homeomorphism)**.** A *homeomorphism* is a continuous function between topological spaces of the same topological type.

Definition 3 (Homomorphism)**.** A *homomorphism* is a structure-preserving map between two algebraic structures of the same type.

We now introduce *first homotopy group*, denoted[2] as $\pi_1(\mathbf{S}, q)$. The group structure of $\pi_1(\mathbf{S}, q)$ determines the topology of $\mathbf{S}$.

1.1 Fundamental Group

Let $\mathbf{S}$ be a two-manifold with a base point $p \in \mathbf{S}$.

Definition 4 (Curve)**.** A *curve* is a continuous mapping $\gamma : [0, 1] \to \mathbf{S}$

[1] The concepts of category and functor were covered in previous lectures

[2] Although the fundamental group in general depends on the choice of base point, it turns out that, up to isomorphism (actually, even up to inner isomorphism), this choice makes no difference as long as the space $\mathbf{S}$ is path-connected. For path-connected spaces, therefore, many authors therefore write $\pi_1(\mathbf{S})$ instead of $\pi_1(\mathbf{S}, q)$

Definition 5 (Loop)**.** A *closed curve* or *loop* through p is a curve s.t. $\gamma(0) = \gamma(1) = p$

Definition 6 (Homotopy)**.** Let $\gamma_0, \gamma_1 : [0,1] \to \mathbf{S}$ be two curves. A *homotopy* connecting γ_0 and γ_1 is a continuous mapping

$$f : [0,1] \times [0,1] \to \mathbf{S}$$

s.t.

$$f(0,t) = \gamma_0(t)$$
$$f(1,t) = \gamma_1(t)$$

We say γ_0 is homotopic to γ_1, if there exists a homotopy between them, denoted as $\gamma_0 \sim \gamma_1$.

Definition 7 (Loop Product)**.** $\gamma_1 \cdot \gamma_2$ is

$$\gamma_1 \cdot \gamma_2(t) := \begin{cases} \gamma_1(2t) & \text{for } 0 \leq t \leq 0.5 \\ \gamma_2(2t-1) & \text{for } 0.5 \leq t \leq 1 \end{cases}$$

Definition 8 (Loop Inverse)**.** $\gamma^{-1}(t) := \gamma(1-t)$

Definition 9 (Fundamental Group)**.** Given a surface topological space $\mathbf{S}$, fix a base point $p \in \mathbf{S}$. Homotopy relation is an equivalence relation[3]. The set of all the loops through the base point p is Γ, which can be classified by homotopy relation and form a set of all the homotopy classes, denoted as $\Gamma/\sim$. To define a group:

- The homotopy class of a loop γ, denoted by $[\gamma]$, becomes group generator.
- The group binary operation is defined as

$$[\gamma_1][\gamma_2] := [\gamma_1 \cdot \gamma_2]$$

  .
- The group unit element is defined as $[e]$, which is as trivial as a point.
- The group inverse element is defined as

$$[\gamma]^{-1} = [\gamma^{-1}]$$

then $\Gamma/\sim$ forms a group, so-called *fundamental group* of $\mathbf{S}$, or the first homotopy group, denoted as $\pi_1(\mathbf{S}, p)$.

Definition 10 (Word Group Representation)**.** Let $G = \{g_1, g_2, ..., g_n\}$ be n distinct symbols. Words of finite length generated by those symbols form a group with equivalence relations

- $\{g_1, g_2, ..., g_n\}$ becomes group generator.
- The group binary operation is defined as the concatenation of two words.

[3] needs to be reflexive, symmetric and transitive

- The group unit element is empty word $\emptyset$
- The group inverse element is defined as.

$$(g_1 g_2 ... g_k)^{-1} = g_k^{-1} ... g_2^{-1} g_1^{-1}$$

- Certain segments of words can be replaced by $\emptyset$, which form equivalence relations, denoted by set $R = \{R_1, R_2, ..., R_m\}$.

Given a set of generators G and a set of relations R, all the equivalence classes of the words generated by G form a group under the concatenation, called *word group*, denoted as

$$\langle g_1, g_2, ..., g_n | R_1, R_2, ..., R_m \rangle$$

Word group representation can be used to process fundamental group in computer.

Theorem 11 (Canonical Representation of Surface Fundamental Group)**.** *Suppose* $\mathbf{S}$ *is a compact, oriented surface,* $p \in \mathbf{S}$ *is a fixed point, the fundamental group has a canonical*[4] *representation*

$$\pi_1(\mathbf{S}, p) = \langle a_1, b_1, a_2, b_2, ..., a_g, b_g | \prod_{i=1}^{g} [a_i, b_i] \rangle$$

where

$$[a_i, b_i] := a_i b_i a_i^{-1} b_i^{-1}$$

and g *is the genus of the surface* $\mathbf{S}$ *and* a_i, b_i *are canonical bases*[5]

Theorem 12. *Topological Spaces Homeomorphism* $\Leftrightarrow$ *Fundamental Groups Isomorphism*

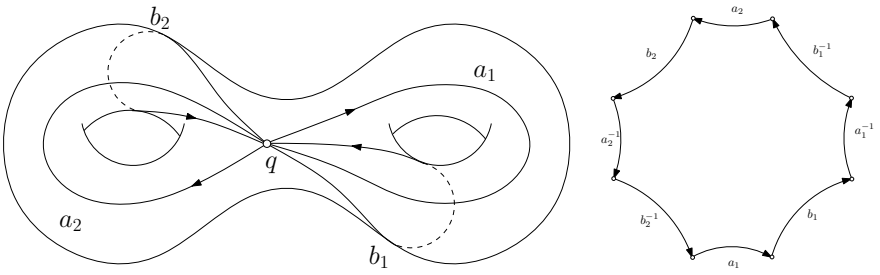

Figure 1.1: fundamental group canonical basis and fundamental domain

Proof. For each surface, find a canonical basis, slice the surface along the basis to get a $4g$ polygonal scheme, then construct a homeomorphism between the polygonal schema with consistent boundary condition. (e.g. bi-torus see figure 1.1) □

[4]The canonical representation of the fundamental group of the surface is not unique. It is NP hard to verify if two given representations are isomorphic.

[5]we omit the definition of canonical basis.

Definition 13 (Connected Sum)**.** The *connected sum* $\mathbf{S}_1 \oplus \mathbf{S}_2$ is formed by deleting the interior of disks $\mathbf{D}_i$ and attaching the resulting punctured surfaces $\mathbf{S}_i - \mathbf{D}_i$ to each other by a homeomorphism $h : \partial\mathbf{D}_1 \to \partial\mathbf{D}_2$

$$\mathbf{S}_1 \oplus \mathbf{S}_2 := (\mathbf{S}_1 - \mathbf{D}_1) \cup_h (\mathbf{S}_2 - \mathbf{D}_2)$$

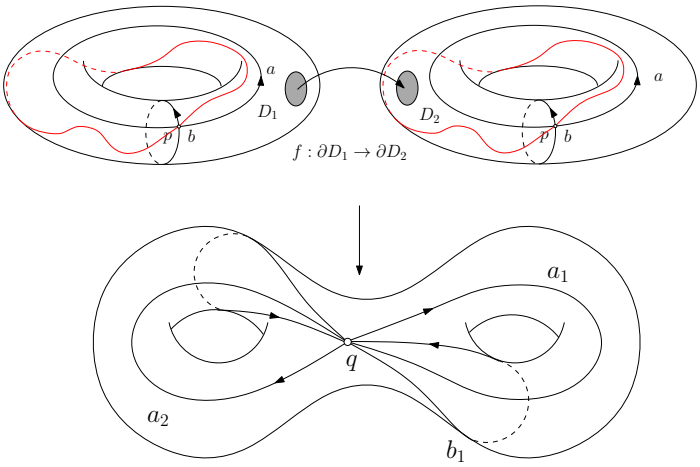

Figure 1.2: connected sum of two tori

Theorem 14 (Classification Theorem of Closed Surfaces)**.** *Any closed connected surface is homeomorphic to exactly one of the following surfaces:*

- *the sphere, a finite connected sum of tori,*
- *the connected sum of g tori for $g \geq 1$*

$$\underbrace{\mathbf{T}^2 \oplus \mathbf{T}^2 \oplus ... \oplus \mathbf{T}^2}_{g \text{ tori}}$$

- *the connected sum of k real projective planes for $k \geq 1$.*

$$\mathbf{RP}^2 \oplus \mathbf{RP}^2 \oplus ... \oplus \mathbf{RP}^2$$

One can use Van Kampen theorem (will be discussed in later course) to show that theorem 11 is true for

$$\mathbf{S} = \oplus_{i=1}^{g} \mathbf{T}^2$$

1.2 Quotient Group

Definition 15 (Coset)**.** Let H be a subgroup of the group G. Given an element g of G,

- the *left cosets* of H in G are the **sets** (not group!) obtained by multiplying each element of H by a fixed element g of G (where g is the left factor), denoted by

$$gH := \{gh : h \in H\}$$

- The *right cosets* are defined similarly, except that the element g is now a right factor, that is,

$$Hg := \{hg : h \in H\}$$

Definition 16 (Normal Subgroup)**.** Subgroup N of group G is *normal subgroup*, denoted as $N \triangleleft G$ if for all g in G, the left cosets gN and right cosets Ng are equal. Notice that any subgroup of an Abelian group is a normal subgroup.

Definition 17 (Quotient Group)**.** Let $N \triangleleft G$. To construct a *quotient group* G/N or $\frac{G}{N}$, N needs to be a normal subgroup of G:

- define the set G/N to be the set of all cosets[6] of N in G. That is, $G/N = \{\underset{a}{N} : a \in G\}$;
- for any two cosets $\underset{a}{N}$ and $\underset{b}{N}$, binary operation $*$ is defined as

$$\underset{a}{N} * \underset{b}{N} = \underset{ab}{N}$$

- the denominator N, the whole normal subgroup, collapsed into the unit[7] element

$$N = \{e\}$$

- the inverse is defined as

$$\underset{a}{N}^{-1} = \underset{a^{-1}}{N}$$

Notice that $G/e = G$ and $G/G = \{e\}$

The concepts of quotient group will be frequently used in following chapters.

1.3 Covering Space

Definition 18 (Covering Space)**.** Given topological spaces $\tilde{\mathbf{S}}$ and $\mathbf{S}$, a continuous map $f : \tilde{\mathbf{S}} \to \mathbf{S}$ is surjective, such that

- for each point $q \in \mathbf{S}$, there is a neighborhood $\mathbf{U}$ of q;
- its preimage $f^{-1}(\mathbf{U}) = \cup_i \tilde{\mathbf{U}}_i$ is a disjoint union of open sets $\tilde{\mathbf{U}}_i$;
- f on each $\tilde{\mathbf{U}}_i$ is a local homeomorphism

[6] since $N \triangleleft G$, left and right cosets coincide, we use $\underset{a}{N}$ to denote coset of N given $a \in G$

[7] In a quotient of a group, the equivalence class of the identity element is always a normal subgroup of the original group, and the other equivalence classes are precisely the cosets of that normal subgroup. We can alternatively think of quotient group as $G/\sim$, where $a \sim b$ if a and b are in the same coset of N

then $(\tilde{\mathbf{S}}, f)$ is a *covering space* of *base space* $\mathbf{S}$, and f is called a projection map.

Definition 19 (Deck Transformation and Covering Group)**.** The automorphisms of $\tilde{\mathbf{S}}$, $g : \tilde{\mathbf{S}} \to \tilde{\mathbf{S}}$, are called *deck transformations*, if they satisfy $f \circ g = f$. All the deck transformations form a group, the *covering group*, and denoted as

$$\text{Deck}(\tilde{\mathbf{S}})$$

Theorem 20 (Covering Group Structure)**.** *Covering space* $\tilde{\mathbf{S}}$ *and base space* $\mathbf{S}$*.*

Suppose base points $\tilde{q} \in \tilde{\mathbf{S}}$*,* $f(\tilde{q}) = q \in \mathbf{S}$*.*

The projection map $f : \tilde{\mathbf{S}} \to \mathbf{S}$ *induces a homomorphism between their fundamental groups*

$$f_* : \pi_1(\tilde{\mathbf{S}}, \tilde{q}) \to \pi_1(\mathbf{S}, q)$$

If $f_*(\pi_1(\tilde{\mathbf{S}}, \tilde{q}))$ *is a normal subgroup of* $\pi_1(\mathbf{S}, q)$ *then the quotient group*

$$\frac{\pi_1(\mathbf{S}, q)}{f_*(\pi_1(\tilde{\mathbf{S}}, \tilde{q}))} \cong \mathit{Deck}(\tilde{\mathbf{S}})$$

Definition 21 (Universal Covering Space)**.** If a covering space $\tilde{\mathbf{S}}$ is simply connected (i.e. $\pi_1(\tilde{\mathbf{S}}) = \{e\}$), then $\tilde{\mathbf{S}}$ is called a *universal covering space* of $\mathbf{S}$.

$$\pi_1(\mathbf{S}) \cong \text{Deck}(\tilde{\mathbf{S}})$$

Namely, the fundamental group of the base space is isomorphic to the deck transformation group of the universal covering space (see figure 1.3)

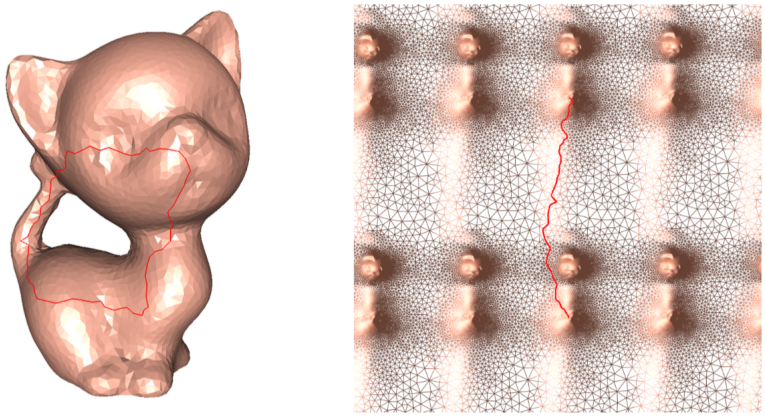

Figure 1.3: base space $\mathbf{S}$ on the left and universal covering space $\tilde{\mathbf{S}}$ on the right

1.4 First Homotopy Group vs. First Homology Group

Homotopy relation does fully capture the topological spaces, but it is hard to compute: the homotopy group is non-Abelian (see figure 1.4). If we can instead represent the topological space by an Abelian group, which can be computed using linear algebra, it would be highly encouraged, even if some loss of information.

By a looser definition of equivalence relation, called homology relation, an Abelian group was formed. The loop product became commutative and therefore was replaced by notation +, called loop formal sum, or just formal sum when generalized to any dimension.

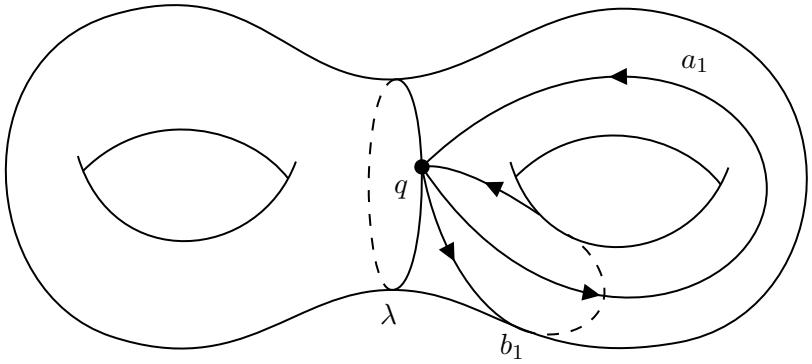

Figure 1.4: In first homotopy group $\pi_1(\mathbf{S}, q)$, we have $[\gamma] = [a_1 b_1 a_1^{-1} b_1^{-1}]$, but $[\gamma] \neq [e]$, so $[a_1][b_1] \neq [b_1][a_1]$, but in first homology group $H_1(\mathbf{S}, \mathbb{Z})$, $[a_1] + [b_1] = [b_1] + [a_1]$, and also we have $[\lambda] = \mathbf{0}$, see example 30

.

Recall definition of *loop product*, which emphasizes the order of concatenation, and therefore it is not commutative. Why don't we just formally sum each parts up, and keep their orientation in record?

Definition 22 (Formal Sum)**.** If an oriented manifold $\mathbf{M}$ can be decomposed into finite simpler submanifolds $\mathbf{m}_1, \mathbf{m}_2, ..., \mathbf{m}_n$ with the same orientation, then we write:

$$\mathbf{M} = \mathbf{m}_1 + \mathbf{m}_2 + ... + \mathbf{m}_n$$

where + denotes *formal sum*. Formal sum is commutative.

Definition 23 (Inverse of Formal Sum)**.** The *inverse of formal sum* of an oriented manifold $\mathbf{M}$ is the sum of inverse of submanifolds $\mathbf{m}_1, \mathbf{m}_2, ..., \mathbf{m}_n$, denoted by "$-$":

$$-\mathbf{M} = -\mathbf{m}_1 - \mathbf{m}_2 - ... - \mathbf{m}_n$$

Definition 24 (Closure)**.** The *closure* of a subset $\mathbf{S}$ of points in a topological space consists of all points in $\mathbf{S}$ together with all limit points of $\mathbf{S}$, denoted by

$$\bar{\mathbf{S}}$$

Definition 25 (Interior)**.** The *interior* of a subset $\mathbf{S}$ of a topological space $\mathbf{X}$ is the union of all subsets of $\mathbf{S}$ that are open in $\mathbf{X}$, denoted by

$$\mathbf{S}^\circ$$

Definition 26 (Boundary and Boundary Operator)**.** The boundary of a subset $\mathbf{S}$ of a topological space $\mathbf{X}$ is the *closure* of $\mathbf{S}$ minus the interior of $\mathbf{S}$:

$$\partial \mathbf{S} := \bar{\mathbf{S}} \setminus \mathbf{S}^\circ$$

We also use $\partial_k \mathbf{\Sigma}$ to indicate that the boundary operator actions on a k-manifold $\mathbf{\Sigma}$.

Example 27 (Boundary of Surface or Loop)**.** For oriented surface, the boundary (loop) is positively oriented "as one walks along boundary on outside surface while cliff on your right". For oriented curve, the boundary are two end-points that the target point is positively oriented and the source point is negatively oriented. We use $\mathbf{0}$ to denote "nothing in space", e.g. the boundary of a sphere or a loop.

Up to this point, to form a group of k-manifolds, we already have:

- commutative binary operation, the *formal sum* "+"
- identity unit element, $\mathbf{0}$, "nothing in space"
- inverse of an element, which is its negatively oriented version.

We need one more thing, the equivalence class, to reveal topological invariant.

Definition 28 (Homology)**.** Let $\mathbf{S}$ be a k-manifold. Let γ_0 and γ_1 be two $(k-1)$-manifolds. A *homology relation* connecting γ_0 and γ_1 is a k-submanifold $\mathbf{\Sigma}$ such that:

$$\partial_k \mathbf{\Sigma} = \gamma_0 - \gamma_1$$

We say γ_0 is homological to γ_1 if there exists homology between them, denoted as $\gamma_0 \sim \gamma_1$ [8].

Definition 29 (First Homology Group)**.** Given a surface topological space $\mathbf{S}$. Homology relation is an equivalence relation. The set of all the loops and finite formal sum of them is $\mathit{\Gamma}$, which can be classified by homology relation and form a set of all the homology classes, denoted as $\mathit{\Gamma}/\sim$. To define a group:

- The homology class of a loop γ, denoted by $[\gamma]$, becomes group generator.
- The group binary operation is defined as

  $$[\gamma_1] + [\gamma_2] := [\gamma_1 + \gamma_2]$$

  which is commutative
- The group unit element is defined as $\mathbf{0}$, which is "nothing in space".
- The group inverse element is defined as

  $$[\gamma]^{-1} = -[\gamma] := [-\gamma]$$

then $\mathit{\Gamma}/\sim$ forms a group, so-called the first homology group, denoted as $H_1(\mathbf{S}, \mathbb{Z})$, if formal sum is over $\mathbb{Z}$, see foot note if over otherwise field[9]

Example 30 (Homology of loops)**.** See figure 1.5, $\mathbf{S}$ is a closed orientable surface with genus $g = 3$. We have formal sum:

[8] Notice that Homotopy $\overset{\not\Leftarrow}{\Rightarrow}$ Homology. To illustrate homology relation is an equivalence relation:

- (reflexive) $\gamma \sim \gamma$ since $\mathbf{0} = \gamma - \gamma$ trivially holds
- (symmetric) if $\gamma_0 \sim \gamma_1$, then $\partial_2 \mathbf{\Sigma} = \gamma_0 - \gamma_1$, then $\partial_2(\mathbf{S} \setminus \mathbf{\Sigma}) = \gamma_1 - \gamma_0$, then $\gamma_1 \sim \gamma_0$
- (transitive) if $\gamma_0 \sim \gamma_1$ and $\gamma_1 \sim \gamma_2$, suppose $\partial_2 \mathbf{\Sigma}_1 = \gamma_0 - \gamma_1$ and $\partial_2 \mathbf{\Sigma}_2 = \gamma_1 - \gamma_2$, then $\partial_2 \mathbf{\Sigma}_1 + \partial_2 \mathbf{\Sigma}_2 = \partial_2(\mathbf{\Sigma}_1 + \mathbf{\Sigma}_2) = \gamma_0 - \gamma_2$ then $\gamma_0 \sim \gamma_2$.

[9] if formal sum over $\mathbb{Z}_2$, for example, then $[\gamma] + [\gamma] = \mathbf{0}$, we denoted first homology group as $H_1(\mathbf{S}, \mathbb{Z}_2)$. If formal sum over $\mathbb{R}$, for example, we allow $0.4[\gamma] - 1.6[\gamma] + \sqrt{2}[\gamma] = (\sqrt{2} - 1.2)[\gamma]$, then denote first homology group as $H_1(\mathbf{S}, \mathbb{R})$

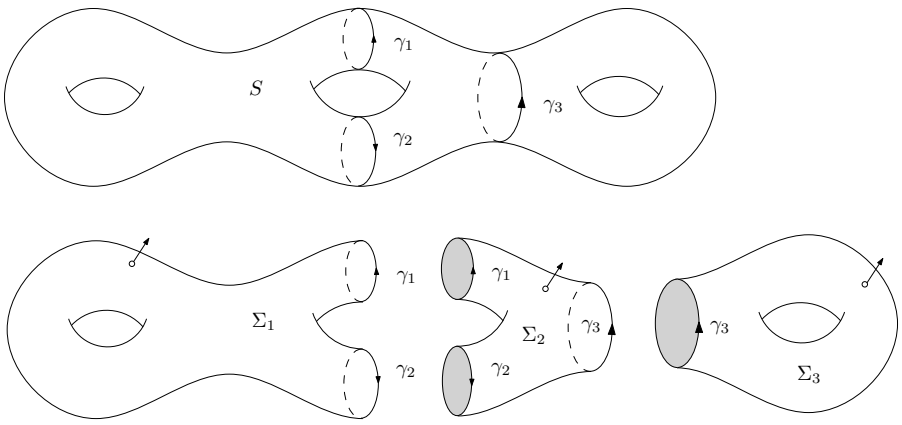

Figure 1.5: an example of homology relation

$$\mathbf{S} = \mathbf{\Sigma}_1 + \mathbf{\Sigma}_2 + \mathbf{\Sigma}_3$$

What can we say about the homological class about γ_1, γ_2 and γ_3? We can see that

$$\gamma_1 \sim \gamma_2 \sim (\gamma_2 + \gamma_3) \sim (\gamma_1 - \gamma_3)$$

$$\gamma_3 \sim (\gamma_1 - \gamma_2) \sim \mathbf{0}$$

since

$$\partial_2 \mathbf{\Sigma}_1 = \gamma_1 - \gamma_2$$

$$\partial_2 \mathbf{\Sigma}_2 = (\gamma_2 + \gamma_3) - \gamma_1 = \gamma_3 - (\gamma_1 - \gamma_2) = \gamma_2 - (\gamma_1 - \gamma_3)$$

$$\partial_2 \mathbf{\Sigma}_3 = \mathbf{0} - \gamma_3$$

1.5 Homology Group

Kernel is the generalization of zeros of a function. Image is the generalization of range of a function.

Definition 31 (Kernel)**.** Let G and H be groups and let $f : G \to H$ be a homomorphism. Let e_H denote the identity unit element in H. The *kernel* of f is defined as

$$\ker f = \{g \in G \mid f(g) = e_H\}$$

Definition 32 (Loop Group)**.** Any closed loop (or finite formal sum of loops) γ on a closed oriented surface $\mathbf{S}$ will satisfy:

$$\partial_1 \gamma = \mathbf{0}$$

We denote *loop group* $Z_1(\mathbf{S})$ as

$$Z_1(\mathbf{S}) = \ker \partial_1 = \{\gamma \in \mathbf{S} \mid \partial_1(\gamma) = \mathbf{0}\}$$

Definition 33 (Image)**.** Let G and H be groups and let $f : G \to H$ be a homomorphism. The *image* of f is defined as

$$\text{img } f = \{h \in H \mid \exists g \in G \ s.t. \ f(g) = h\}$$

Definition 34 (Boundary Group)**.** Any submanifold $\mathbf{\Sigma}$ on a closed oriented surface $\mathbf{S}$ will induce a closed boundary γ:

$$\partial_2 \mathbf{\Sigma} = \gamma$$

We denote *boundary group* $B_1(\mathbf{S})$ as

$$B_1(\mathbf{S}) = \text{img } \partial_2 = \{\gamma \in \mathbf{S} \mid \exists \mathbf{\Sigma} \in \mathbf{S} \ s.t. \ \partial_2 \mathbf{\Sigma} = \gamma\}$$

Definition 35 (Homology Group Structure)**.** The first homology group of $\mathbf{S}$ is the quotient group

$$H_1(\mathbf{S}, \mathbb{Z}) = \frac{Z_1(\mathbf{S})}{B_1(\mathbf{S})} = \frac{\ker \partial_1}{\text{img } \partial_2}$$

Which is consistent with homology relation, as we collapse $B_1(\mathbf{S})$ as identity (all $\partial_2 \mathbf{\Sigma}$ now become $\mathbf{0}$)

Generally, given $(k+1)$-manifold $\mathbf{M}$, k homology group is

$$H_k(\mathbf{M}, \mathbb{Z}) = \frac{Z_k(\mathbf{M})}{B_k(\mathbf{M})} = \frac{\ker \partial_k}{\text{img } \partial_{k+1}}$$

Figure 1.6 illustrates the relationship between groups:

- C_k, which is group of all k-submanifold
- Z_k, which is group of kernel of ∂_k on k-submanifold
- B_k, which is group of image of ∂_{k+1} on $(k+1)$-submanifold

$$B_k(\mathbf{M}) \subset Z_k(\mathbf{M}) \subset C_k(\mathbf{M})$$

and

$$\partial_k \circ \partial_{k+1} = \mathbf{0}$$

Theorem 36. *Suppose* $\mathbf{S}$ *is a path-connected genus* g *closed surface, then*

$$H_0(\mathbf{S}, \mathbb{Z}) \cong \mathbb{Z} \cong H_2(\mathbf{S}, \mathbb{Z})$$

$$H_1(\mathbf{S}, \mathbb{Z}) \cong \mathbb{Z}^{2g}$$

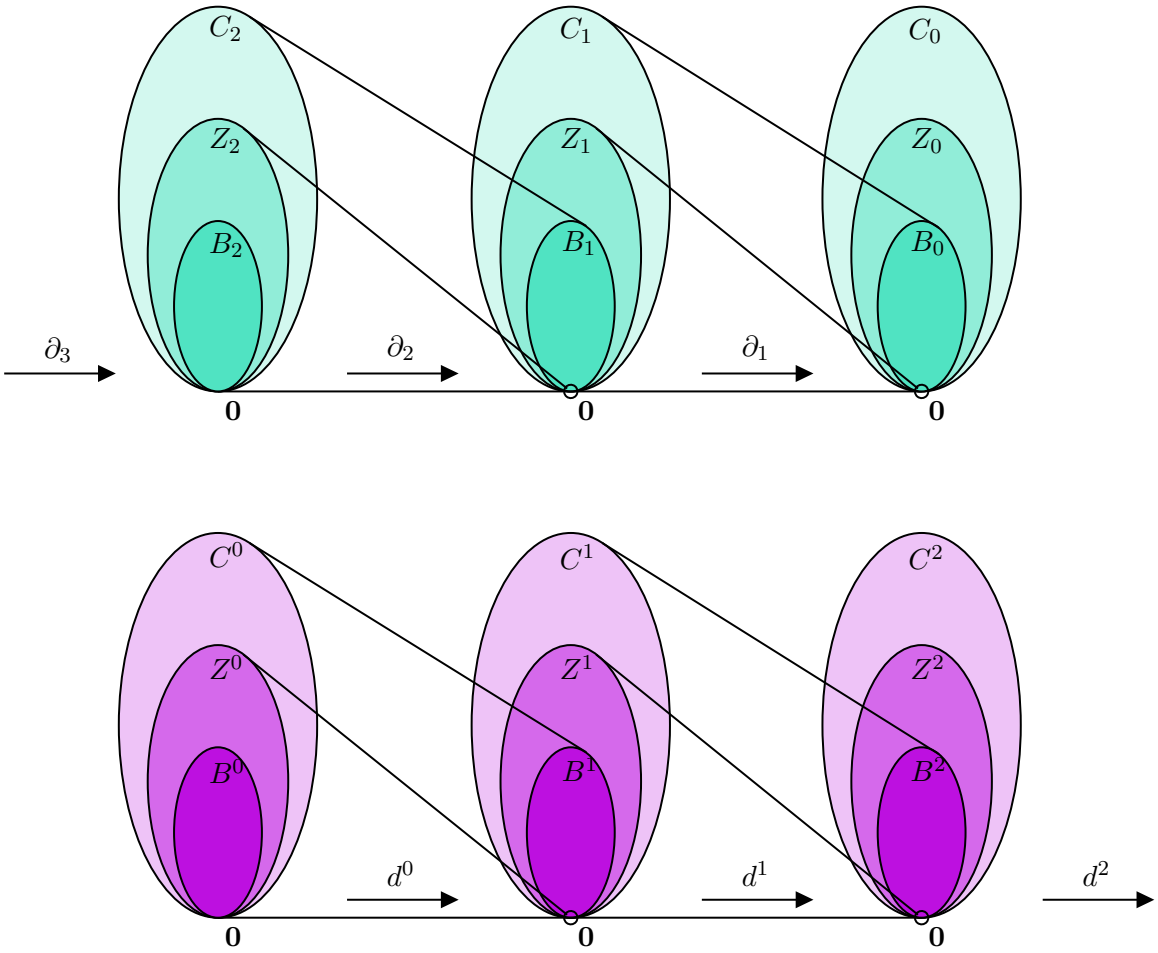

Figure 1.6: The relation of groups C_k, Z_k and B_k, and their duality, C^k, Z^k and B^k

1.6 First Homology Group vs. First Cohomology Group

We have another Abelian group that can encode the same topological information of homology group but can be computed even faster. However, few people understand. We would like to point out *k-form* is the generalization of function, and *coboundary operator* is the generalization of gradient. Before we get there, we now introduce some concept in differential geometry, which would be frequently used.

Definition 37 (Tangent Space)**.** Given a point x on closed surface $\mathbf{M}$, a *tangent space* of $\mathbf{M}$ through x, denoted as

$$T_x\mathbf{M}$$

is a vector space of plane that contains the possible directions in which one can tangentially pass through x. The elements of the *tangent space* $T_x\mathbf{M}$ at x are called the *tangent vectors* v at x, see figure 1.7:

Definition 38 (Tangent Bundle)**.** The *tangent bundle* of a differentiable manifold $\mathbf{M}$ is a manifold $T\mathbf{M}$ which assembles all the tangent vectors in $\mathbf{M}$, given by the disjoint union of the tangent spaces of $\mathbf{M}$:

$$T\mathbf{M} := \bigcup_{x\in\mathbf{M}} \{x\} \times T_x\mathbf{M} = \bigcup_{x\in\mathbf{M}} \{(x,v) \mid v \in T_x\mathbf{M}\} = \{(x,v) \mid x \in \mathbf{M}, v \in T_x\mathbf{M}\}$$

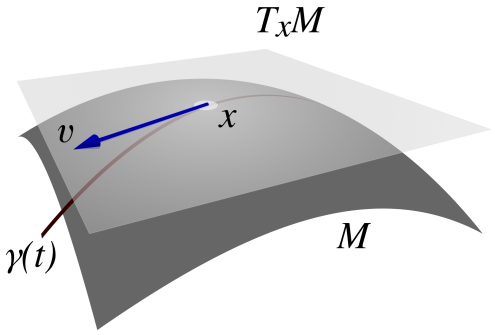

Figure 1.7: The tangent space $T_x\mathbf{M}$ and a tangent vector v on $T_x\mathbf{M}$, along a curve $\gamma(t)$ traveling through $x \in \mathbf{M}$

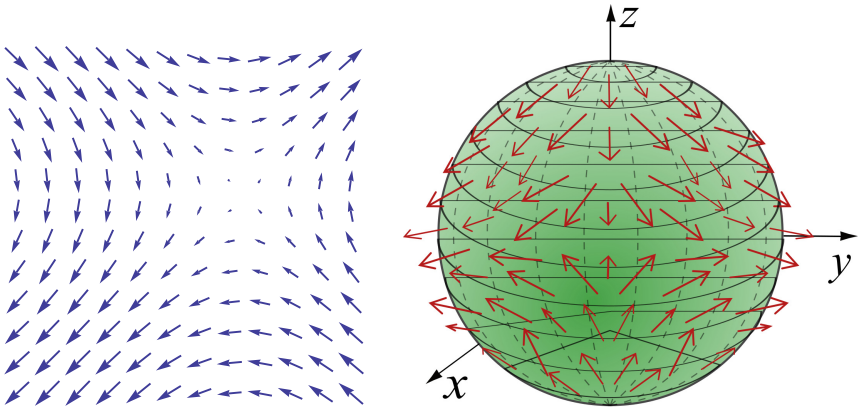

Figure 1.8: Vector field $f : \mathbf{D} \to \mathbb{R}^2$ (left) and $g : \mathbf{S} \to T\mathbf{S}$ (right)

Definition 39 (Vector Field)**.**

A *vector field* on the region $\mathbf{D} \subset \mathbb{R}^2$ is a vector-valued function

$$f : \mathbf{D} \to \mathbb{R}^2$$

A *vector field* on a surface $\mathbf{S}$ is an assignment of a tangent vector to each point in $\mathbf{S}$. More precisely, a mapping from $\mathbf{S}$ to tangent bundle of $\mathbf{S}$:

$$g : \mathbf{S} \to T\mathbf{S}$$

See figure 1.8

Definition 40 (Line Integral)**.** Integration of vector field F along a curve is called *line integral*.

$$\int_\gamma F(v) \cdot dv$$

or simply denoted as

$$\langle F, \gamma \rangle$$

Definition 41 (Curl Free Vector Field)**.** A *curl free field* F of is a vector field such that the line integral along any **loop** γ equals zero:

$$\oint_\gamma F(v) \cdot dv = 0$$

or written as

$$\text{curl } F = 0$$

Definition 42 (Gradient Vector Field)**.** A *gradient field* (or *conservative field*) F is a vector field such that the line integral along any **boundary** γ equals zero:

$$\oint_{\gamma} F(v) \cdot dv = 0$$

or equivalently we say that there exist a scalar field φ that its gradient is F:

$$F = \nabla\varphi \quad \text{or} \quad F = \text{grad } \varphi$$

Notice that just like boundary $\overset{\Leftarrow}{\Rightarrow}$ loop

$$\text{gradient field} \overset{\Leftarrow}{\Rightarrow} \text{curl free field}$$

Definition 43 (1-form)**.** Given an oriented closed surface $\mathbf{S}$, a *1-form* f of $\mathbf{S}$ encoded by a vector field F on $\mathbf{S}$ is a linear mapping from any curve $\gamma \in C_1(\mathbf{S})$ to line integral $\langle F, \gamma\rangle \in \mathbb{R}$:

$$f : C_1(\mathbf{S}) \to \mathbb{R}$$

we write:

$$f(\gamma) = \langle f, \gamma\rangle := \langle F, \gamma\rangle$$

Since the *1-form* of $\mathbf{S}$ is very much of the vector filed F, so people use *vector field* and *1-form* interchangeably. Recall that group of any curve $C_1(\mathbf{S})$, group of loops $Z_1(\mathbf{S})$ and group of boundaries $B_1(\mathbf{S})$ with

$$B_1(\mathbf{S}) \subset Z_1(\mathbf{S}) \subset C_1(\mathbf{S})$$

since

$$\text{boundary} \overset{\Leftarrow}{\Rightarrow} \text{loop}$$

Now we consider another way to describe such topological information.

Definition 44 (First Cohomology Group)**.** Given a surface topological space $\mathbf{S}$. We define three groups of 1-form (vector field) with binary operation "+" over $\mathbb{Z}$, unit element 0 and inverse as "-" prefix:

- group of all vector field over $\mathbf{S}$, denoted as

$$C^1(\mathbf{S})$$

- curl free field group, denoted as $Z^1(\mathbf{S})$

$$Z^1(\mathbf{S}) = \{f \in C^1(\mathbf{S}) \mid \langle f, \gamma\rangle = 0,\ \gamma \in Z_1(\mathbf{S})\}$$

- gradient field group, denoted as $B^1(\mathbf{S})$

$$B^1(\mathbf{S}) = \{f \in C^1(\mathbf{S}) \mid \langle f, \gamma\rangle = 0,\ \gamma \in B_1(\mathbf{S})\}$$

Since

$$\text{boundary} \overset{\text{生}}{\Rightarrow} \text{loop}$$

We have

$$B^1(\mathbf{S}) \subset Z^1(\mathbf{S}) \subset C^1(\mathbf{S})$$

The *first cohomology group* $H^1(\mathbf{S}, \mathbb{Z})$ is achieved by collapsing $B^1(\mathbf{S})$ into identity:

$$H^1(\mathbf{S}, \mathbb{Z}) = \frac{Z^1(\mathbf{S})}{B^1(\mathbf{S})}$$

and notice that

$$H^1(\mathbf{S}, \mathbb{Z}) \cong H_1(\mathbf{S}, \mathbb{Z})$$

Until now, we may not have proper language to describe what is a cohomology relation, although we derive cohomology group. What does it mean if f_0 is cohomologous to f_1?

A scalar field φ on $\mathbf{S}$ is a 0-form. By gradient operator, it becomes a vector field F, the 1-form. Imagine any of tiny oriented curve γ on $\mathbf{S}$. The gradient can be thought of the difference of the scalar values of two end points, which is the summation of 0-form of boundary of the curve (because boundary will give one positive and one negative value):

$$\underbrace{F}_{\text{1-form}} = \underbrace{\text{grad} \overbrace{\varphi}^{\text{0-form}}}_{\text{1-form}} = \underbrace{\varphi \circ \partial}_{\text{1-form}}$$

Now the generalization of gradient by relating boundary operator is coboundary operator

Definition 45 (Coboundary and Coboundary Operator)**.** k-dimensional *Coboundary operator* d^k actions on a k-form f:

$$d^k f(\cdot) := f \circ \partial_{k+1}(\cdot)$$

we say $d^k f$, a $(k+1)$-form, is the coboundary of f, the k-form.

Notice that

$$d^k \circ d^{k-1}(\cdot) = 0$$

holds for any input of $(k-1)$-manifold. In the case of $d^1 \circ d^0(\cdot)$, namely, the curl of gradient is zero.

We also derive

Theorem 46 (Stokes Theorem)**.**

$$\langle dw, \sigma \rangle = \langle w, \partial\sigma \rangle$$

Definition 47 (Cohomology)**.** Let $\mathbf{S}$ be a surface topological space. Let f_0 and f_1 be two k-forms. A *cohomology relation* connecting f_0 and f_1 is a $(k-1)$-form φ such that:

$$d^{k-1}\varphi = f_0 - f_1$$

We say that f_0 is cohomologous to f_1 if there exists such $(k-1)$-form φ, denoted as $f_0 \sim f_1$, and cohomology class $[f_0] = [f_1]$.

Definition 48 (Cohomology Group Structure)**.** We omit further details, see figure 1.6:

$$H^k(\mathbf{S}, \mathbb{Z}) = \frac{Z^k(\mathbf{S})}{B^k(\mathbf{S})} = \frac{\ker d^k}{\text{img } d^{k-1}}$$

Theorem 49 (Poincaré Duality)**.** *Given n dimensional topological space* $\mathbf{S}$*:*

$$H^k(\mathbf{S}, \mathbb{Z}) \cong H_{n-k}(\mathbf{S}, \mathbb{Z})$$

When $n = 2$ as in the case of surface topology, given path-connected oriented closed genus g surface $\mathbf{S}$, we have

$$H^2(\mathbf{S}, \mathbb{Z}) \cong H_0(\mathbf{S}, \mathbb{Z}) \cong \mathbb{Z} \cong H_2(\mathbf{S}, \mathbb{Z}) \cong H^0(\mathbf{S}, \mathbb{Z})$$

$$H^1(\mathbf{S}, \mathbb{Z}) \cong H_1(\mathbf{S}, \mathbb{Z}) \cong \mathbb{Z}^{2g}$$

Definition 50 (Dual Cohomology Basis)**.** suppose a homology basis of $H_1(\mathbf{S})$ is $\{\gamma_1, \gamma_2, ..., \gamma_n\}$, the *dual cohomology basis* is $\{w_1, w_2, ..., w_n\}$, satisfying:

$$\langle w_i, \gamma_j \rangle = 1_{i=j}$$

where

$$1_{\mathcal{A}} := \begin{cases} 1 & \text{if } \mathcal{A} \text{ is true} \\ 0 & \text{otherwise} \end{cases}$$

Chapter 2

Basic Discrete Surface Algebraic Topology

The discrete version of algebraic surface topology was built on oriented 2-dimensional simplicial complex, namely the triangular mesh, which was implemented by half-edge data structure in computer.

2.1 Half-edge Data Structure

Definition 51 (Half-edge Data Structure)**.** The *half-edge* data structure of triangular mesh approximating an oriented surface has the following classes:

V *vertex* class

H *half-edge* class, oriented from one vertex (the *source* vertex) to another vertex (the *target* vertex)

E *edge* class, each edge has two opposite half-edges, with the exception that the edge on boundary only has one half-edge

F *face* class, each face has three half-edges, oriented counter-clockwisely with respect to the normal of face

with the following pointer functions which take in the realization of classes above:

$v(\cdot)$ vertex pointer function $v : \mathbf{H} \to \mathbf{V}$ parametrized by "source/target" that points a half-edge to a vertex. $v_{\text{sour}}(\cdot)$ points to the source vertex, and $v_{\text{targ}}(\cdot)$ points to the target vertex

$f(\cdot)$ face pointer function $f : \mathbf{H} \to \mathbf{F}$ that points a half-edge to a face that it belongs to

$e(\cdot)$ edge pointer function $e : \mathbf{H} \to \mathbf{E}$ that points a half-edge to an edge that it belongs to

$h(\cdot)$ the polymorphic half-edge pointer function can recognize different inputs and take different actions:

half-edge $h : \mathbf{H} \to \mathbf{H}$ parametrized by "next/previous" that points a half-edge to another half-edge, where $h_{\text{next}}(\cdot)$ points to the next half-edge, and $h_{\text{prev}}(\cdot)$ points to the previous half-edge

face $h : \mathbf{F} \to \mathbf{H}$ points a face to the *first* half-edge it contains

vertex $h : \mathbf{V} \to \mathbf{H}$ points a vertex to the *first* half-edge that the vertex was targeted

edge $h : \mathbf{E} \to \mathbf{H} \times \mathbf{H}$ points an edge to the pair of half-edges it contains (with exception of boundary edge that has only one half-edge, in that case $h : \mathbf{E} \to \mathbf{H}$)

Example 52 (2-chain)**.** As shown in figure 2.1, we have realization of classes:

$$\mathbf{V} = \{v_1, v_2, v_3, v_4, v_5, v_6\} =: v_{1:6}$$
$$\mathbf{H} = h_{1:12}$$
$$\mathbf{E} = e_{1:9}$$
$$\mathbf{F} = f_{1:4}$$

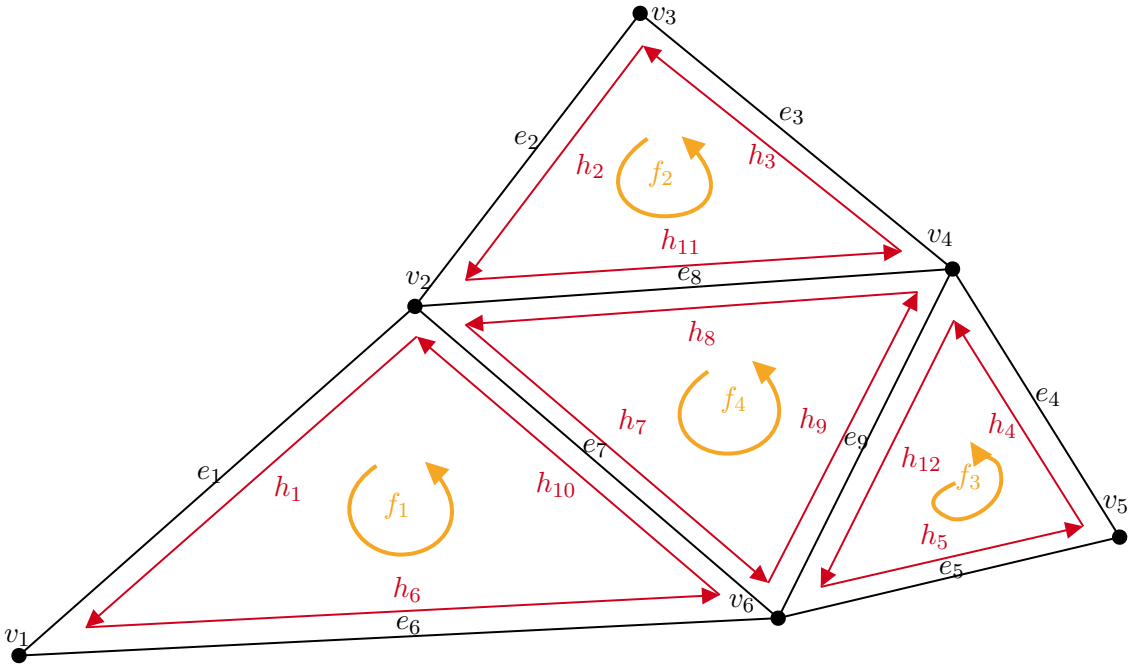

Figure 2.1: an example of half-edge data structure of a simplicial complex $\mathbf{\Sigma} = f_1 + f_2 + f_3 + f_4$

and pointer functions :

1. $v(\cdot)$ is obvious to every half-edge in the picture, e.g. $v_{\text{sour}}(h_1) = v_2$ and $v_{\text{targ}}(h_1) = v_1$
2. $f(\cdot)$ is also obvious to every face in the picture, e.g. $f(h_1) = f(h_6) = f(h_{10}) = f_1$
3. $e(\cdot)$ in this picture is:

$$e(h_n) = \begin{cases} e_n & \text{if } n \leq 9 \\ e_{n-3} & \text{otherwise} \end{cases}$$

4. $h(\cdot)$ in this picture, firstly

$$h(e_n) = \begin{cases} h_n & \text{if } e_n \text{ on boundary} \\ (h_n, h_{n+3}) & \text{otherwise} \end{cases}$$

secondly we denote e.g. $h_{\text{next}}(h_1) = h_6$ and $h_{\text{prev}}(h_6) = h_1$ as $1 \to 6$, then we denote all $h : \mathbf{H} \to \mathbf{H}$ as

$$1 \to 6 \to 10 \to 1 \qquad 2 \to 11 \to 3 \to 2 \qquad 4 \to 12 \to 5 \to 4 \qquad 8 \to 7 \to 9 \to 8$$

thirdly we set "the first half-edge" of each face and fourthly "the first half-edge" of each target vertex in this picture (note that these are merely arbitrary choices) as follows:

$$h(f_1) = h_1 \quad h(f_2) = h_2 \quad h(f_3) = h_5 \quad h(f_4) = h_8$$
$$h(v_n) = h_n$$

Now we rephrase example 52 in discrete surface topology language.

2.2 Discrete Algebraic Surface Topology

Definition 53 (Simplex)**.** Suppose $k+1$ linear independent points embedded in $\mathbb{R}^n$

$$v_0, v_1, ..., v_k$$

the standard *k-simplex*

$$[v_0, v_1, ..., v_k]$$

is the minimal convex set including all of them.

e.g. in figure 52, the 2-simplex (vertices written counter-clock-wisely)

$$f_1 = [v_2, v_1, v_6]$$

the 1-simplex (vertices written from source to target)

$$h_1 = [v_2, v_1]$$

Definition 54 (Simplicial Complex)**.** A *simplicial complex* $\mathbf{\Sigma}$ is an union of simplicies with "vertex auto -alignment".

Example 55 (Simplicial Complex)**.** See figure 2.2

Definition 56 (Chain)**.** A *k-chain* is **a linear combination (formal sum)** of all k-simplicies in $\mathbf{\Sigma}$.

Definition 57 (Chain Space)**.** The *k-dimensional chain space* is the linear space formed by all k-chain by formal sum over $\mathbb{Z}$, denoted as

$$C_k(\mathbf{\Sigma}, \mathbb{Z})$$

e.g. in figure 52,

- in $C_2(\mathbf{\Sigma}, \mathbb{Z})$, a 2-chain could be f_1, $f_1 + f_2$, or even $f_1 + 3f_2 - 4f_3$

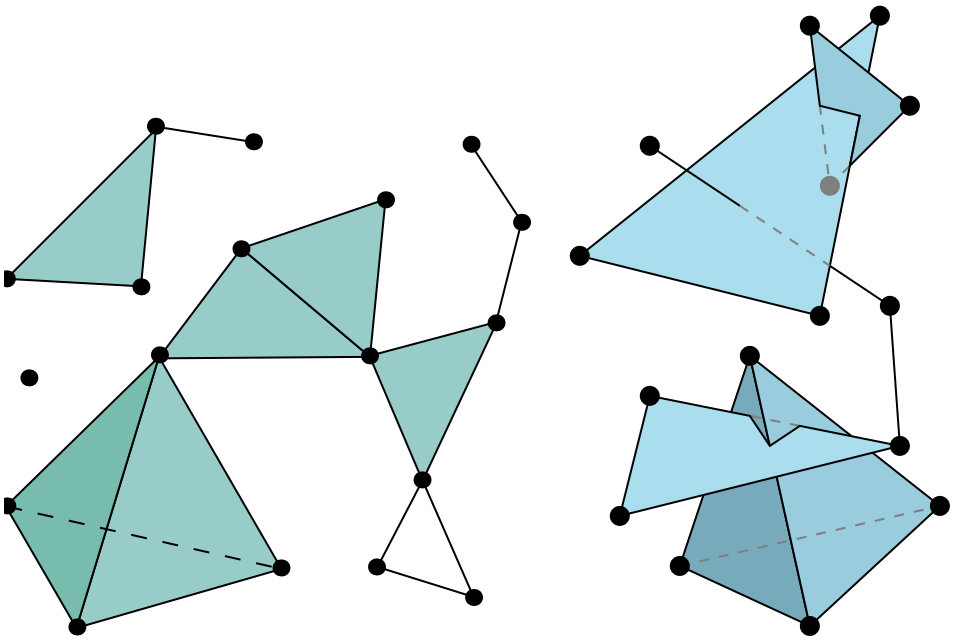

Figure 2.2: An example (left) and not-example (right) of simplicial complex

- in $C_1(\mathbf{\Sigma}, \mathbb{Z})$, a 1-chain could be $h_1 + h_2$, or even $2h_1 - 5h_2 + 3h_4$

Definition 58 (Boundary Operator)**.** The discrete version of boundary operator ∂, could be implemented as follows: we use hat notation as we delete $\hat{v_i}$ from $[v_0, ..., \hat{v_i}, ..., v_k]$. Then

$$\partial[v_0, v_1, ..., v_k] = \sum_{i=0}^{k} (-1)^i [v_0, ..., \hat{v_i}, ..., v_k]$$

e.g. in figure 52,

- $\partial f_2 = \partial[v_3, v_2, v_4] = [v_3, v2] + [v_2, v_4] - [v_3, v_4] = h_2 + h_{11} + h_3$
- $\partial h_1 = \partial[v_2, v_1] = v_1 - v_2$

we would easily see that the boundary operator is linear, e.g.

$$\partial \mathbf{\Sigma} = \partial(f_1 + f_2 + f_3 + f_4) = \partial f_1 + \partial f_2 + \partial f_3 + \partial f_4$$

and $\partial^2 = \mathbf{0}$, e.g.

$$\partial^2 f_2 = \partial(h_2 + h_{11} + h_3) = v_2 - v_3 + v_4 - v_2 + v_3 - v_4 = \mathbf{0}$$

Definition 59 (Cochain Space)**.** By assigning a value to each k-simplex (opposite half-edges get same value with different symbols), one can get a *k-dimensional cochain space* formed by all k-cochain, which takes in a k-chain and outputs the summation of value of k-simplicies of the k-chain.

We define discrete version:

$$\begin{aligned} \text{closed 1-chain} &\longleftrightarrow \text{loop} \\ \text{exact 1-chain} &\longleftrightarrow \text{boundary} \\ \text{closed 1-cochain} &\longleftrightarrow \text{curl free field} \\ \text{exact 1-cochain} &\longleftrightarrow \text{gradient field} \end{aligned}$$

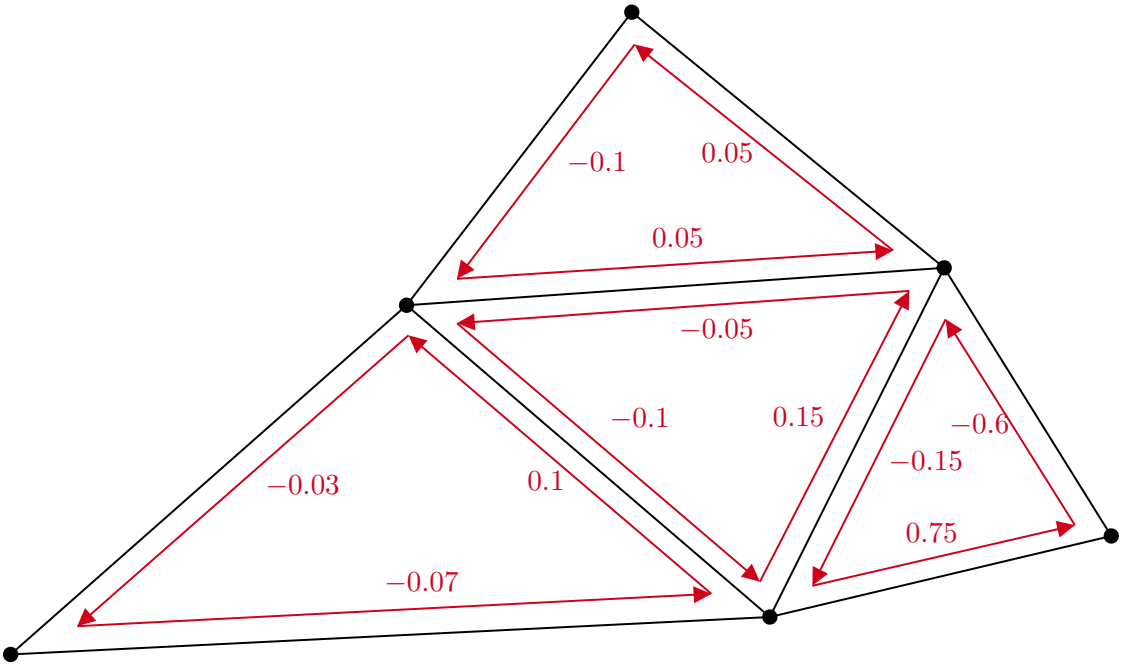

Figure 2.3: an example of 1-cochain w constructed from $\mathbf{\Sigma}$

Example 60 (1-cochain)**.** see figure 2.3, we have

$$w(h_2 + h_7) = w(h_2) + w(h_7) = -0.1 - 0.1 = -0.2$$

and one can see that any exact 1-chain γ in $\mathbf{\Sigma}$, we have

$$w(\gamma) = 0$$

so w is an exact 1-cochain.

Recall that *graph* $G = (V, E)$, by its definition, is contained in a simplicial complex $\mathbf{\Sigma}$.

Definition 61 (Dual Graph)**.** The *dual graph* $\bar{G}$ of a plane graph G, is a graph that

- has a vertex for each face of G
- has an edge whenever two faces of G are separated from each other by an edge, and a self-loop when the same face appears on both sides of an edge

Thus, each edge e of G has a corresponding dual edge $\bar{e}$ in $\bar{G}$, whose endpoints are the dual vertices corresponding to the faces on either side of e.

Definition 62 (Spanning Tree)**.** A *spanning tree* T of an undirected graph G is a subgraph that is a tree which includes all of the vertices of G, with a minimum possible number of edges.

2.3 Algorithms of $\pi_1(\mathbf{\Sigma})$, $\tilde{\mathbf{\Sigma}}$, $H_1(\mathbf{\Sigma})$ and $H^1(\mathbf{\Sigma})$

We now introduce algorithms to compute

- $\pi_1(\mathbf{\Sigma})$, first homotopy group of $\mathbf{\Sigma}$ (algorithm 1)
- $\tilde{\mathbf{\Sigma}}$, universal covering space $\mathbf{\Sigma}$ (algorithm 2)
- $H_1(\mathbf{\Sigma})$, first homology group of $\mathbf{\Sigma}$ (algorithm 3)
- $H^1(\mathbf{\Sigma})$, first cohomology group of $\mathbf{\Sigma}$ (algorithm **??**)

represented by 1-chain or 1-cochain as group basis. For computation of the first homology group $H_1(\mathbf{\Sigma})$, it has the same bases with the first homotopy group $\pi_1(\mathbf{\Sigma})$. However, it is not the case in higher dimensions. For higher dimensional computation of homology group basis, please consult eigen-decomposition of combinatorial Laplace operator using Smith norm.

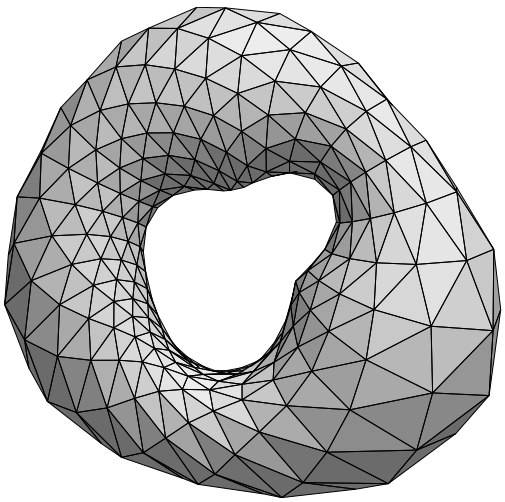

Figure 2.4: a triangulation mesh on a genus 1 surface

Algorithm 1: First Homotopy Group $\pi_1(\mathbf{\Sigma})$

Input: a closed triangular mesh $\mathbf{\Sigma}$
Output: $\pi_1(\mathbf{\Sigma})$

1. compute the dual mesh $\bar{\mathbf{\Sigma}}$ of the input mesh $\mathbf{\Sigma}$
2. compute a spanning tree $\bar{\mathbf{T}}$ of $\bar{\mathbf{\Sigma}}$, rooted at an arbitrary point p
3. the *cut graph* $\mathbf{\Gamma}$ of $\mathbf{\Sigma}$ is given by
$$\mathbf{\Gamma} := \{e \in \mathbf{\Sigma} \mid \bar{e} \notin \bar{\mathbf{T}}\}$$
4. compute a spanning tree $\mathbf{T}$ of $\mathbf{\Gamma}$
5. select an edge $e_i \in \mathbf{\Gamma} \setminus \mathbf{T}$, then $e_i \cup \mathbf{T}$ gives an unique closed 1-chain γ_i; suppose we get a set of distinct 1-chains
$$\{\gamma_1, \gamma_2, ..., \gamma_k\}$$
which is the set of generators of $\pi_1(\mathbf{\Sigma})$
6. cut the mesh $\mathbf{\Sigma}$ along $\mathbf{\Gamma}$ to obtain $\tilde{\mathbf{\Sigma}}_0$, the fundamental domain of $\mathbf{\Sigma}$
7. set $R = \emptyset$, let $\gamma = \partial\tilde{\mathbf{\Sigma}}_0$, traverse γ, once $e_i^{\pm 1}$ is encountered, append $\gamma_i^{\pm 1}$ to R,
$$R \leftarrow R\gamma_i^{\pm 1}$$
8. the first homotopy group of $\mathbf{\Sigma}$
$$\pi_1(\mathbf{\Sigma}, p) = \langle \gamma_1, \gamma_2, ..., \gamma_k \mid R \rangle$$

Algorithm 2: Universal Covering Space $\tilde{\mathbf{\Sigma}}$

Input: a closed triangular mesh $\mathbf{\Sigma}$
Output: an universal covering space $\tilde{\mathbf{\Sigma}}$ with desired size

1. the same as step 1 $\rightarrow$ 6 in algorithm 1
2. set $\tilde{\mathbf{\Sigma}} = \tilde{\mathbf{\Sigma}}_0$, glue a copy of $\tilde{\mathbf{\Sigma}}_0$ with $\tilde{\mathbf{\Sigma}}$ along γ_i, a homeomorphism $h : \partial\tilde{\mathbf{\Sigma}} \supset \gamma_i \sim \gamma_i^{-1} \subset \partial\tilde{\mathbf{\Sigma}}_0$
$$\tilde{\mathbf{\Sigma}} \leftarrow \tilde{\mathbf{\Sigma}} \cup_h \tilde{\mathbf{\Sigma}}_0$$
3. trace the boundary of $\tilde{\mathbf{\Sigma}}$, if there are two adjacent 1-chains $\gamma_j, \gamma_{j+1} \subset \partial\tilde{\mathbf{\Sigma}}$, such that $\gamma_j^{-1} = \gamma_{j+1}$ then glue them together
4. repeat step 2 and step 3, until $\tilde{\mathbf{\Sigma}}$ is large enough

Algorithm 3: First Homology Group $H_1(\mathbf{\Sigma})$

Input: a closed triangular mesh $\mathbf{\Sigma}$
Output: $H_1(\mathbf{\Sigma})$

1. the same as step $1 \to 5$ in algorithm 1
2. $H_1(\mathbf{\Sigma}) = \{[\gamma_1], [\gamma_2], ..., [\gamma_{2g}]\}$

Algorithm 4: First Cohomology Group $H^1(\mathbf{\Sigma})$

Input: a closed triangular mesh $\mathbf{\Sigma}$
Output: $H^1(\mathbf{\Sigma})$

1. the same as step $1 \to 2$ in algorithm 3
2. for each γ_i, slice $\mathbf{\Sigma}$ along γ_i to obtain a mesh $\mathbf{\Sigma}_i$ with two boundaries. We have $\partial\mathbf{\Sigma}_i = \gamma_i^+ - \gamma_i^-$
3. set a 0-form τ_i on $\mathbf{\Sigma}_i$ such that $\tau_i(v^+) = 1$ for all vertices $v^+ \in \gamma_i^+$ and $\tau_i(v^-) = 0$ for all vertices $v^- \in \gamma_i^-$; set $w_i = d\tau_i$
4. $H^1(\mathbf{\Sigma}) = \{[w_1], [w_2], ..., [w_{2g}]\}$

Chapter 3

Maps between Topological Spaces

Definition 63 (Continuous Map)**.** A *continuous map* f is a continuous function between two topological spaces $\mathbf{M}$ and $\mathbf{N}$, denoted as,

$$f : \mathbf{M} \to \mathbf{N}$$

Definition 64 (Simplicial Map)**.** A *simplicial map* φ between simplicial complexes K and L is a function

$$\varphi : \mathrm{Vert}(K) \to \mathrm{Vert}(L)$$

from the vertex set of K, to that of L such that whenever $v_0, v_1, ..., v_q$ span a q-simplex of K, $\varphi(v_0), \varphi(v_1), ..., \varphi(v_q)$ span a p-simplex ($p \leq q$) of L. Of course, repetitions among $\varphi(v_0), \varphi(v_1), ..., \varphi(v_q)$ are allowed.

Note that the simplicial map φ can be regarded as a function from K to L: this function sends a simplex σ of K with vertices $v_0, v_1, ..., v_q$ to the simplex $\varphi(\sigma)$ of L spanned by vertices $\varphi(v_0), \varphi(v_1), ..., \varphi(v_q)$, so we also write φ as

$$\varphi : K \to L$$

Note that the simplicial map φ also induces a continuous map

$$\varphi : |K| \to |L|$$

between $|K|$ and $|L|$ (the polyhedra[1] of K and L), where a point inside $|K|$ spanned by vertex $v_0, v_1, ..., v_q$ is sent to a point inside $|L|$ continuously by

$$\varphi\left(\sum_{j=0}^{q} t_j v_j\right) = \sum_{j=0}^{q} t_j \varphi(v_j) \quad \text{whenever} \quad 0 \leq t_j \leq 1 \quad \text{for} \quad j = 0, 1, ..., q \quad \text{and} \quad \sum_{j=0}^{q} t_j = 1$$

As a closing remark, there are thus three equivalent ways of describing a simplicial map:

[1] $|K|$ always denotes the polyhedra of simplicial complex K.

- for 0-simplex σ_0, $|\sigma_0|$ is itself
- for 1-simplex σ_1, $|\sigma_1|$ is itself
- for 2-simplex σ_2, $|\sigma_2|$ is the triangle it contains
- for 3-simplex σ_3, $|\sigma_3|$ is the tetrahedron it contains

1. as a function between the vertex sets of two simplicial complexes, e.g. $\varphi : \mathrm{Vert}(K) \to \mathrm{Vert}(L)$
2. as a function from one simplicial complex to another, e.g. $\varphi : K \to L$
3. as a continuous map between the polyhedra of two simplicial complexes, e.g. $\varphi : |K| \to |L|$

We shall describe a simplicial map using the representation that is most appropriate in the given context.

3.1 Simplicial Approximation Theorem

One may have experience with **Minecraft** game or **Lego** toy. Any real world object can be discretized in lattice. The mathematical theorem behind is *simplicial approximation theorem*, which guarantees that a continuous manifold can be (by a slight deformation) approximated by a simplicial complex of the simplest kind given its embedded simplicial complex space.

Example 65 (Manifold Embedded in Simplicial Complex)**.** See figure 3.1, The manifold $\mathbf{M}$ embedded in a given simplicial complex L described by a continuous map from $|K|$, the "parameter", to $|L|$:

$$\mathbf{M} : |K| \to |L|$$

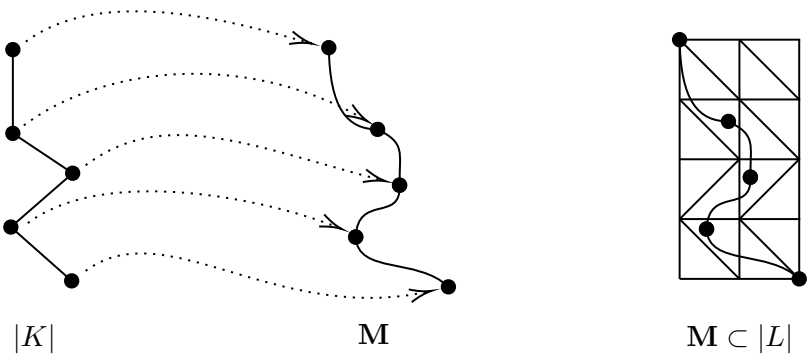

Figure 3.1: manifold $\mathbf{M}$ was represented by a continuous map: $\mathbf{M} : |K| \to |L|$

Definition 66 (Star of a Vertex)**.** Let K be a simplicial complex and let $p \in \mathrm{Vert}(K)$. Then the *star* of p, the "discrete version of the neighbor of a point", denoted by $\mathrm{st}(p)$, is defined by

$$\mathrm{st}(p) = \bigcup s^\circ \subset |K| \quad \text{where simplex} \quad s \in K \quad \text{such that} \quad p \in \mathrm{Vert}(s)$$

Example 67 (Star of a Vertex)**.** As shown in figure 3.2, $\mathrm{st}(p)$ consists of the open shaded region, all the open simplices of which p is a neighbor.

Definition 68 (Simplicial Approximation)**.** Let $\mathbf{M}$ be a manifold represented by a continuous map $\mathbf{M} : |K| \to |L|$. Its approximating candidate $\mathbf{M}_\Delta$, represented by a

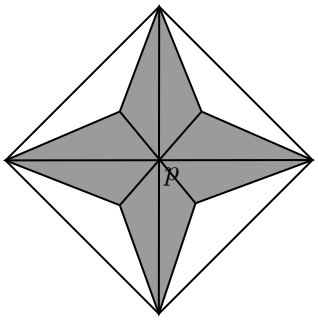

Figure 3.2: star of p, denoted by $\mathrm{st}(p)$

simplicial map $\mathbf{M}_\Delta : K \to L$, is *simplicial approximation* to $\mathbf{M}$ if, for every vertex p of K,

$$\mathbf{M}(\mathrm{st}(p)) \subset \mathrm{st}(\mathbf{M}_\Delta(p))$$

which means $\mathbf{M}$ carries neighboring simplices of p inside the union of the simplices near $\mathbf{M}_\Delta(p)$. $\mathbf{M}_\Delta$ and $\mathbf{M}$ are close up to a meshing unit.

Example 69 (Simplicial Approximation)**.** See figure 3.3, $\mathbf{M}_\Delta$ is an simplicial approximation to $\mathbf{M}$. $\mathbf{M}_\Delta$ (red) is the simplest approximation to $\mathbf{M}$, achieved by $\mathrm{Sd}^1 K$, the *first-order barycentric subdivision* of K. Barycentric subdivision and simplicial approximation theorem will be explained right away.

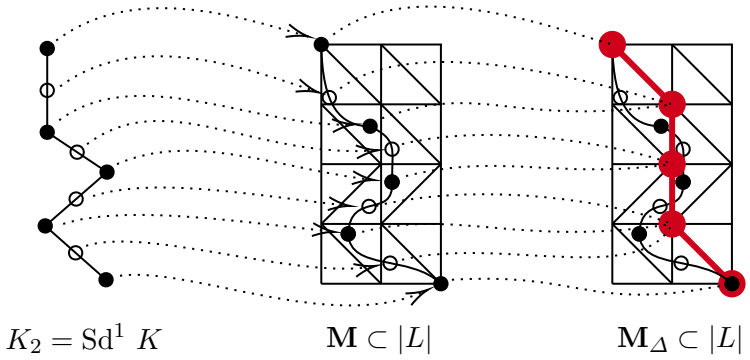

Figure 3.3: The simplicial approximation theorem guarantees that a simplest approximation in a given embedding mesh will be achieved by sufficient iterations of barycentric subdivision of "parameter".

Definition 70 (Barycentric Subdivision)**.** If s is a simplex, let b^s denote its barycenter. If K is a simplicial complex, define $\mathrm{Sd}\ K$, the *barycentric subdivision* of K, to be the simplicial complex with

$$\mathrm{Vert}(\mathrm{Sd}\ K) = \{b^s : s \in K\}$$

note that here $s \in K$ are simplex of all dimensions in K. Recall that if s is a 0-simplex then trivially $b^s = s$; if s is a 1-simplex then b^s is the central point of two vertices; and so on. The q times iteration of barycentric subdivision is denoted by

$$\mathrm{Sd}^q K$$

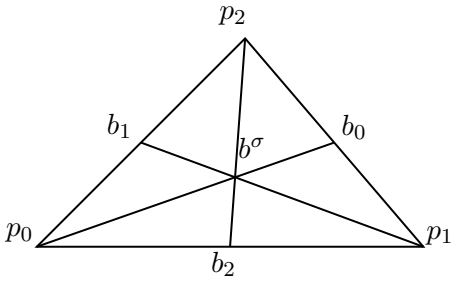

Figure 3.4: first order barycentric subdivision of the simplex σ

Example 71 (Barycentric Subdivision)**.** See figure 3.4, if simplex $\sigma = [p_0, p_1, p_2]$, then $\text{Vert}(\text{Sd } \sigma) = \{p_0, p_1, p_2, b_0, b_1, b_2, b^\sigma\}$.

Definition 72 (Simplicial Approximation Theorem)**.** Given simplicial complexes K and L. A smooth manifold $\mathbf{M}$ represented by continuous map $\mathbf{M} : |K| \to |L|$ must have a simplicial approximation, and could be found its simplest kind after some barycentric subdivision of K by

$$\mathbf{M}_\Delta : \text{Sd}^q K \to L \quad \text{where} \quad q \geq 1$$

Simplicial approximation theorem was the foundation of modern movie industry and game industry, since it provides a theoretical guarantee that the simplest discrete digital approximation of any smooth-shaped object exists.

Example 73 (Simplicial Approximation Theorem)**.** See figure 3.1, one cannot construct a simplicial approximation to $\mathbf{M}$ by its "parameter" K, but one can do so by K_2, the first-order barycentric subdivision of "parameter", as shown in figure 3.3

3.2 Chern-Gauss-Bonnet Theorem

Definition 74 (Induced Maps)**.** Algebraic topology constructs functor

$$\mathfrak{C}_1 \to \mathfrak{C}_2$$

between $\mathfrak{C}_1 = \{\text{Topological Spaces, Homeomorphisms}\}$ and $\mathfrak{C}_2 = \{\text{Groups, Homomorphisms}\}$. Therefore, a continuous map $f : \mathbf{M} \to \mathbf{N}$ naturally induces homomorphism. there basically two kinds of *induced map*:

- *push-forward map*, denoted by $f_\#$ if on homotopy, and denoted by f_* if on homology.

  $f_\#$ maps between fundamental groups[2] :

  $$f_\# : \pi_1(\mathbf{M}) \to \pi_1(\mathbf{N})$$

[2] $f_\#$ takes "curves" to "curves":

$$f_\# : C_p(\mathbf{M}) \to C_p(\mathbf{N})$$

$f_\#$ takes "cycles" to "cycles":

$$f_\# : Z_p(\mathbf{M}) \to Z_p(\mathbf{N})$$

$f_\#$ takes "boundaries" to "boundaries":

$$f_\# : B_p(\mathbf{M}) \to B_p(\mathbf{N})$$

f_* maps between p^{th}-homology groups, where p should be clear in the context:

$$f_* : H_p(\mathbf{M}) \to H_p(\mathbf{N})$$

- *pull-back map*, denoted as f^* if it maps between p^{th}-cohomology groups[3], where p should be clear in the context:

$$f^* : H^p(\mathbf{N}) \to H^p(\mathbf{M})$$

Example 75 (Induced Maps of Surface)**.** Suppose $\mathbf{M}$ and $\mathbf{N}$ are two closed surfaces, a continuous map:

$$f : \mathbf{M} \to \mathbf{N}$$

induces a push-forward map on first homology:

$$f_* : H_1(\mathbf{M}) \to H_1(\mathbf{N})$$

and a pull-back map on first cohomology:

$$f^* : H^1(\mathbf{N}) \to H^1(\mathbf{M})$$

Suppose a curve $\sigma \in C_1(\mathbf{M}) \subset H_1(\mathbf{M})$ and a vector field $\omega \in C^1(\mathbf{N}) \subset H^1(\mathbf{M})$, then

$$\omega[f_*(\sigma)] = [f^*(\omega)](\sigma)$$

Definition 76 (Degree of a Map)**.** Suppose $\mathbf{M}$ and $\mathbf{N}$ are two closed surfaces, the *degree of map* of a continuous map $f : \mathbf{M} \to \mathbf{N}$ is the algebraic number[4] of pre-images $f^{-1}(q)$ for arbitrary point $q \in \mathbf{N}$, denoted by $\deg(f)$, which is independent of the choice of the point q. A quick example see figure 3.5

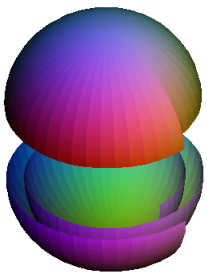

Figure 3.5: a continuous map $f : \mathbf{M} \to \mathbf{M}$ from a sphere to itself but in 2x speed. For every point $q \in \mathbf{M}$, there are two pre-images, so $\deg(f) = 2$

[3]here we explain why push-forward and pull-back are opposite direction in a natural way.

- Points are sent forward. Given $p \in \mathbf{M}$ we have $f(p) \in \mathbf{N}$
- Functions are sent back, i.e. pull back from $\mathbf{N}$ to $\mathbf{M}$. If we have a function $\omega : \mathbf{N} \to \mathbb{R}$ then we get the composition $\omega \circ f : \mathbf{M} \to \mathbb{R}$. The pull back can be considered a *functional* map, which maps from function on $\mathbf{N}$ to function on $\mathbf{M}$

[4]if Jacobian at that point q is positive then count +1, otherwise then count -1, then degree of map is sum of total count

Example 77 (Degree of a Map)**.** Suppose $\mathbf{M}$ and $\mathbf{N}$ are two closed surfaces, a continuous map:

$$f : \mathbf{M} \to \mathbf{N}$$

induces a push-forward map on second homology:

$$f_* : H_2(\mathbf{M}) \to H_2(\mathbf{N})$$

since $H_2(\mathbf{M}, \mathbb{Z}) \cong \mathbb{Z} \cong H_2(\mathbf{N}, \mathbb{Z})$, we also write its isomorphism:

$$\tilde{f}_* : \mathbb{Z} \to \mathbb{Z}$$

and it must have the form

$$\tilde{f}_*(z) = \deg(f) \cdot z$$

Definition 78 (Euler-Poincaré Characteristic)**.** let g be the genus of a closed surface $\mathbf{S}$, then *Euler characteristic*, denoted as $\chi(\mathbf{S})$, is

$$\chi(\mathbf{S}) = 2(1 - g)$$

the discrete version, if $\mathbf{S}$ triangulated in $\mathbf{S}_\Delta$, is

$$\chi(\mathbf{S}_\Delta) = |\text{Faces}| - |\text{Edges}| + |\text{Vertices}|$$

Definition 79 (Gaussian Curvature)**.** At any point on a surface, we can find a normal vector that is at right angles to the surface; planes containing the normal vector are called normal planes. The intersection of a normal plane and the surface will form a curve called a normal section and the curvature of this curve is the normal curvature. For most points on most surfaces, different normal sections will have different curvatures; the maximum and minimum values of these are called the principal curvatures, call these κ_1, κ_2. The *Gaussian curvature* is the product of the two principal curvatures $K = \kappa_1 \cdot \kappa_2$, as shown in figure 3.6

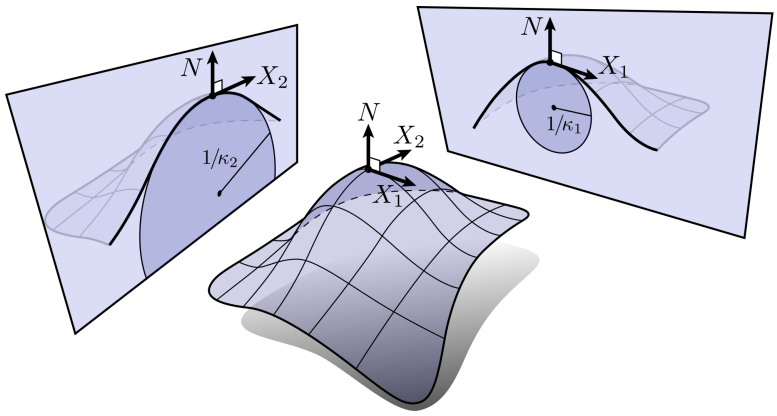

Figure 3.6: Gaussian curvature is the product of principal curvature κ_1 and κ_2. The curvature of a circle is reciprocal of radius: $1/r$. So if the curvature is κ, the radius is $1/\kappa$, as noted in the figure

Theorem 80 (Chern-Gauss-Bonnet Theorem)**.** *Let $\boldsymbol{S}$ be a closed surface, $K(p)$ the Gaussian curvature at point p on surface, and $dA(p)$ the element area at point p on surface, then its total Gaussian curvature*

$$\int_{\boldsymbol{S}} K(p)dA(p) = 2\pi\chi(\boldsymbol{S})$$

Shiing-Shen Chern provided simple intrinsic proof of Gauss-Bonnet Theorem, which added his name to Gauss-Bonnet. We illustrate his beautiful proof by applying degree of Gauss map and homotopy between surfaces.

proof. consider the Gauss Map $G : \mathbf{S}^* \to \mathbb{S}^2$ from a canonical closed surface $\mathbf{S}^*$ to unit sphere $\mathbb{S}^2$. Whenever a point p on surface with normal $\mathbf{n}(p)$, the Gauss Map maps it to a point $G(p)$ on unit sphere with the same normal $\mathbf{n}(p)$.

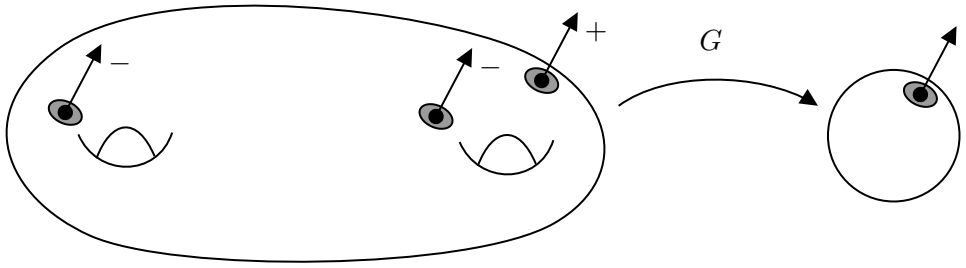

Figure 3.7: The canonical shape of genus g closed surface $\mathbf{S}^*$ can guarantee $\deg(G) = 1-g$ since the count of pre-image is strictly negative whenever a hole appears.

"canonical" here means it guarantees

$$\deg(G) = 1 - g$$

so the total area of the image of $\mathbf{S}^*$ on unit sphere $\mathbb{S}^2$ is

$$\text{Area}(\mathbb{S}^2) \times \deg(G) = 4\pi \deg(G) = 4\pi(1-g) = 2\pi\chi(\mathbf{S}^*)$$

Note that the total area of the image of $\mathbf{S}^*$ on unit sphere $\mathbb{S}^2$ also equals to

$$\int_{\mathbf{S}^*} \frac{\text{Area}(G(p))}{\text{Area}(p)} dA(p)$$

which equals to, since it is a Gauss Map[5]:

$$\int_{\mathbf{S}^*} \frac{\text{Area}(G(p))}{\text{Area}(p)} dA(p) = \int_{\mathbf{S}^*} K(p)dA(p)$$

thus we get, for a canonical closed surface $\mathbf{S}^*$, the identity

$$\int_{\mathbf{S}^*} K(p)dA(p) = 2\pi\chi(\mathbf{S}^*)$$

[5]for Gauss Map, when shrinking a patch around point p, its limit is Gaussian curvature:

$$\lim_{\Omega_p \to 0} \frac{\text{Area}(G(\Omega_p))}{\text{Area}(\Omega_p)} = K(p)$$

Now consider the quantity

$$\frac{\int_{\mathbf{S}^*} K(p)dA(p)}{2\pi} = \chi(\mathbf{S}^*) \in \mathbb{Z}$$

is an integer, which should not change under continuous deformation from canonical shaped $\mathbf{S}^*$ to any closed surface $\mathbf{S}$ with same genus g, thus we get for any closed surface $\mathbf{S}$

$$\int_{\mathbf{S}} K(p)dA(p) = 2\pi\chi(\mathbf{S})$$

□

Example 81 (Chern-Gauss-Bonnet Theorem)**.** let $\mathbf{S}$ be a sphere with radius R, its genus $g = 0$, then $\chi(\mathbf{S}) = 2 \times (1 - 0) = 2$, its Gaussian curvature is constant $\frac{1}{R^2}$, according to Chern-Gauss-Bonnet formula

$$\int_{\mathbf{S}} \frac{1}{R^2} dA(p) = \frac{1}{R^2} \int_{\mathbf{S}} dA(p) = \frac{1}{R^2} \times \text{Area}(\mathbf{S}) = 2\pi\chi(\mathbf{S}) = 4\pi$$

indeed $\text{Area}(\mathbf{S}) = 4\pi R^2$.

3.3 Fixed Point Theorem

Definition 82 (Inclusion Map)**.** an *inclusion map* i from A to B, where $A \subset B$, satisfies that for any element $x \in A$ we have $i(x) = x$, denoted as

$$i : A \hookrightarrow B$$

Theorem 83 (Brouwer's Fixed Point Theorem)**.** *Suppose $\Omega \subset \mathbb{R}^n$ is a compact convex set, $f : \Omega \to \Omega$ is a continuous map, then there exists a point $p \in \Omega$ such that*

$$f(p) = p$$

proof. Assume $f : \Omega \to \Omega$ has no fixed point, namely

$$\forall p \in \Omega, \quad f(p) \neq p$$

We can construct $g : \Omega \to \partial\Omega$, a ray starting from $f(p)$ through p and intersect $\partial\Omega$ at $g(p)$. Because our assumption $f(p) \neq p$ and Ω is convex, g is well-defined. Note that if point $p \in \partial\Omega$ then $g(p) = p$, as shown in figure 3.8. We construct an inclusion map $i : \partial\Omega \hookrightarrow \Omega$, which maps a point $p \in \partial\Omega$ to itself. Then we compose it with g,

$$\partial\Omega \overset{i}{\hookrightarrow} \Omega \overset{g}{\to} \partial\Omega$$

we get an identity map:

$$(g \circ i) : \partial\Omega \to \partial\Omega$$

which induces a push-forward map on $(n-1)^{th}$ homology:

$$(g \circ i)_* : H_{n-1}(\partial\Omega, \mathbb{Z}) \to H_{n-1}(\partial\Omega, \mathbb{Z})$$

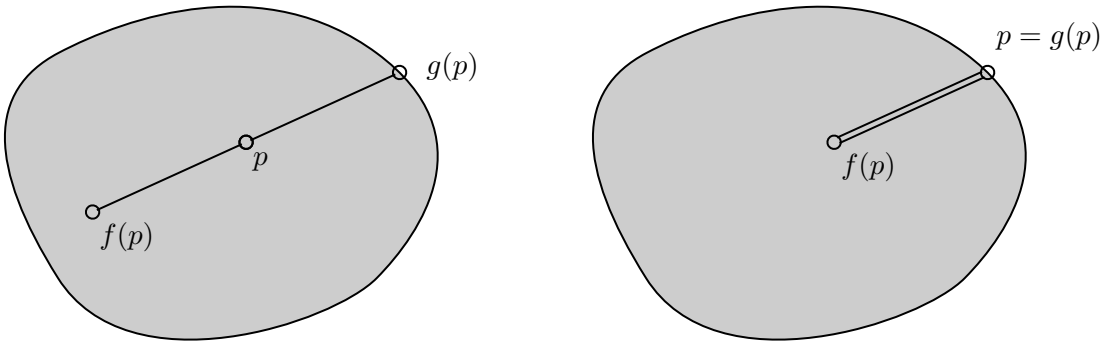

Figure 3.8: diagram of $g : \Omega \to \partial\Omega$ (left) and $(g \circ i) : \partial\Omega \to \partial\Omega$ (right)

since it is identity map,

$$(g \circ i)_* : z \mapsto z$$

$g : \Omega \to \partial\Omega$ induces a push-forward map on $(n-1)^{th}$ homology:

$$g_* : H_{n-1}(\Omega, \mathbb{Z}) \to H_{n-1}(\partial\Omega, \mathbb{Z})$$

however, since Ω is compact convex set

$$H_{n-1}(\Omega, \mathbb{Z}) = 0, \quad g_* = 0$$

so

$$(g \circ i)_* = g_* \circ i_* = 0$$

contradiction! $f : \Omega \to \Omega$ has fixed point. □

In 1910, Luitzen Egbertus Jan Brouwer proved his fixed point theorem, which ensured the existence of fixed point of a continuous self-map of convex compact space. Often, it can be stated as follow:

Example 84 ("Swirling Coffee" Theorem)**.** Use a stick (volume can be ignored) to swirl a cup of coffee without making any bubble. In the end, there is a molecule with final position the same as initial position in your coffee.

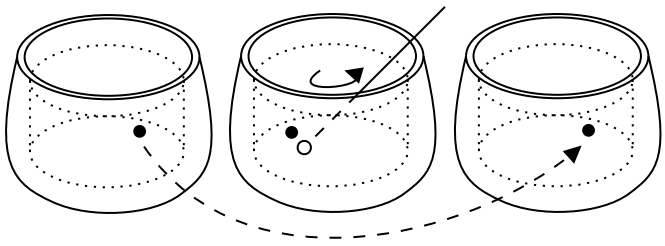

Figure 3.9: "swirling coffee" theorem: at least one molecule, "doesn't move" before and after coffee swirling

In 1926, Solomon Lefschetz gave a formula that relates the number of fixed points of a map to the induced push-forward maps on homology.

Definition 85 (Index of Fixed Point)**.** Suppose $\mathbf{M}$ is an n-dimensional topological space, p is a fixed point of self-map $f : \mathbf{M} \to \mathbf{M}$. Choose a neighborhood $\mathbf{U}$ such that $p \in \mathbf{U} \subset \mathbf{M}$, consider the boundary of $\mathbf{U}$, which is a $(n-1)$-dimensional $\partial\mathbf{U}$. Similar to the concept "degree of a map" (see example 77), the induced push-forward map on $(n-1)^{th}$ homology:

$$f_* : H_{n-1}(\partial\mathbf{U}, \mathbb{Z}) \to H_{n-1}(\partial\mathbf{U}, \mathbb{Z})$$

is $f_* : \mathbb{Z} \to \mathbb{Z}$ and must have the form $f_* : z \mapsto \lambda z$, where λ is an integer called the *algebraic index of fixed point* p of map f, denoted as

$$\mathrm{Ind}(f, p) = \lambda$$

Definition 86 (Trace of Self-map)**.** Let $\mathbf{A}$ be a matrix representing a self-map $f : \mathbf{M} \to \mathbf{M}$ under any basis, then the *trace* of f, denoted as

$$\mathrm{Tr}(f)$$

is $\mathrm{Tr}(\mathbf{A})$, the trace of $\mathbf{A}$, which is independent of choice of basis.

Definition 87 (Lefschetz-Hopf Fixed Point Formula)**.** Given compact topological space $\mathbf{M}$. The sum of indices of all fixed points of a self-map $f : \mathbf{M} \to \mathbf{M}$ equals to the alternating sum of trace of push-forward map on k^{th} homology $f_{*k} : H_k(\mathbf{M}, \mathbb{Z}) \to H_k(\mathbf{M}, \mathbb{Z})$ induced by the self-map f

$$\sum_{p \in \mathrm{Fix}(f)} \mathrm{Ind}(f, p) = \sum_k (-1)^k \mathrm{Tr}(f_{*k}) =: \Lambda(f)$$

where $\Lambda(f)$ is called *Lefschetz number*, and $\mathrm{Fix}(f)$ denotes the set of all fixed points of f

Example 88 (Lefschetz-Hopf Fixed Point Formula)**.** consider a simple self-map $f : [0, 1] \to [0, 1]$. we have

$$\Lambda(f) = \underbrace{\mathrm{Tr}(f_{*0} : \mathbb{Z} \to \mathbb{Z})}_{1} - \underbrace{\mathrm{Tr}(f_{*1} : 0 \to 0)}_{0} = 1 = \sum_{p \in \mathrm{Fix}(f)} \mathrm{Ind}(f, p)$$

as shown in figure 3.10

Theorem 89 (Lefschetz's Fixed Point Theorem)**.** *Given a continuous self-map of a compact topological space $f : \boldsymbol{M} \to \boldsymbol{M}$, if its Lefschetz number $\Lambda(f) \neq 0$, then there is a point $p \in \boldsymbol{M}$ such that*

$$f(p) = p$$

Proof (Advanced). Notation update:

- f_k: the induced push-forward map on k-dimensional space
- $f_k \mid C_k$: the induced map on k-chain group
- $f_k \mid H_k$: the induced map on k-homology
- $\oplus$: direct sum between groups, e.g. $A \oplus B = \{(a + b) \mid a \in A, b \in B\}$

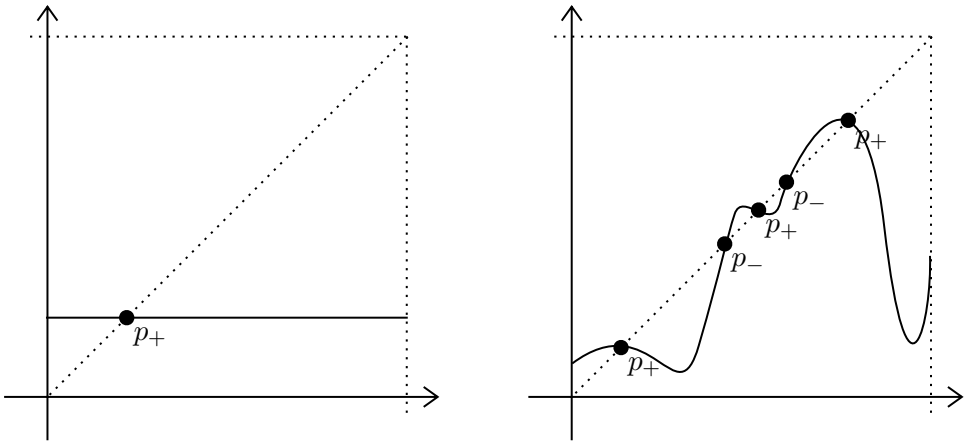

Figure 3.10: a self-map $f_1 : [0,1] \to \text{const}$ (left) versus its homotopic self-map f_2 with same Lefshcetz number $\Lambda(f_1) = \Lambda(f_2) = 1$

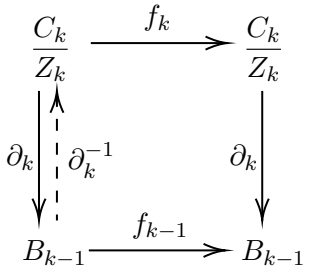

Figure 3.11: commutative diagram of induced map and boundary operator

According to simplicial approximation theorem, there must be approximated maps up to any precision. So we triangulate $\mathbf{M}$ first, and assume its induced map f can be both embedded in chain space and smooth space, as shown in the commutative diagram as figure 3.11:

we have

$$(f_{k-1} \mid B_{k-1}) = \partial_k \circ (f_k \mid \frac{C_k}{Z_k}) \circ \partial_k^{-1}$$

and thus

$$\begin{aligned} \mathrm{Tr}(f_{k-1} \mid B_{k-1}) &= \mathrm{Tr}([\partial_k][f_k \mid \frac{C_k}{Z_k}][\partial_k^{-1}]) \\ &= \mathrm{Tr}([f_k \mid \frac{C_k}{Z_k}][\partial_k^{-1}][\partial_k]) \\ &= \mathrm{Tr}(f_k \mid \frac{C_k}{Z_k}) \end{aligned}$$

according to property of trace.

Let C_k be k-chain group, Z_k closed chain group, B_k exact chain group, H_k homology group. We have

$$C_k \cong \frac{C_k}{Z_k} \oplus Z_k \qquad \text{and} \qquad Z_k \cong B_k \oplus H_k$$

thus

$$\begin{aligned}\mathrm{Tr}(f_k \mid C_k) &= \mathrm{Tr}(f_k \mid \frac{C_k}{Z_k} \oplus Z_k) \\ &= \mathrm{Tr}(f_k \mid \frac{C_k}{Z_k}) + \mathrm{Tr}(f_k \mid Z_k) \\ &= \mathrm{Tr}(f_{k-1} \mid B_{k-1}) + \mathrm{Tr}(f_k \mid B_k) + \mathrm{Tr}(f_k \mid H_k)\end{aligned}$$

thus

$$\sum_k (-1)^k \mathrm{Tr}(f_k \mid C_k) = \sum_k (-1)^k [\overbrace{\mathrm{Tr}(f_{k-1} \mid B_{k-1}) + \mathrm{Tr}(f_k \mid B_k)}^{\text{cancel out in sequence}} + \mathrm{Tr}(f_k \mid H_k)] \quad (3.1)$$

$$= \sum_k (-1)^k \mathrm{Tr}(f_k \mid H_k) \quad (3.2)$$

$$= \Lambda(f) \quad (3.3)$$

according to Lefschetz-Hopf fixed point formula. Whenever $\Lambda(f) \neq 0$, there is an entry in a matrix such that $\mathrm{Tr}(f_k \mid C_k) \neq 0$, which means there is simplex $\sigma \in C_k$ such that $f_k(\sigma) \subset \sigma$, for any point in $|\sigma|$, the continuous map $f_k : |\sigma| \to |\sigma|$ must have a Brouwer's fixed point such that $f_k(p) = p$, which means

$$f(p) = p$$

□

Example 90 (Lefschetz Number, Betti Number and Euler-Poincaré Characteristic)**.** Consider an identity map of a closed surface

$$\mathrm{id} : \mathbf{S} \to \mathbf{S}$$

the identity map is, of course, a self-map. According to equations 3.1, 3.2 and 3.3, we have

$$\begin{aligned}\Lambda(\mathrm{id}) = \sum_k (-1)^k \mathrm{Tr}(\mathrm{id}_k \mid C_k) &= \underbrace{\mathrm{Tr}(\mathrm{id}_2 \mid C_2)}_{|\text{Faces}|} - \underbrace{\mathrm{Tr}(\mathrm{id}_1 \mid C_1)}_{|\text{Edges}|} + \underbrace{\mathrm{Tr}(\mathrm{id}_0 \mid C_0)}_{|\text{Vertices}|} \\ = \sum_k (-1)^k \mathrm{Tr}(\mathrm{id}_k \mid H_k) &= \underbrace{\mathrm{Tr}(\mathrm{id}_2 \mid H_2)}_{b_2} - \underbrace{\mathrm{Tr}(\mathrm{id}_1 \mid H_1)}_{b_1} + \underbrace{\mathrm{Tr}(\mathrm{id}_0 \mid H_0)}_{b_0} \\ &= \chi(\mathbf{S})\end{aligned}$$

Here we show that for an identity map, the connection between its Lefschetz number and Euler-Poincaré characteristic, and where Euler (number of triangulation elements) and Poincaré (Betti number) coincide.

Geometrically, Betti number of surface can be understood as:

- b_0 is the number of connected components
- b_1 is the number of one-dimensional or "circular" holes
- b_2 is the number of two-dimensional "voids" or "cavities"

e.g. for a tours, $b_0 = 1$, $b_1 = 2$ and $b_2 = 1$

3.4 Poincaré-Hopf Theorem

Lefschetz-Hopf fixed point formula directly leads to Poincaré-Hopf index theorem, which relates the number of zeros of a vector field to the topological invariant of space where the vector field is embedded.

Definition 91 (Isolated Zero Point)**.** Given a smooth vector field on a surface $\mathbf{S}$

$$v_{\mathbf{S}} : \mathbf{S} \to T\mathbf{S}$$

assigning each point $p \in \mathbf{S}$ a tangent vector $v_{\mathbf{S}}(p) \in T\mathbf{S}$, then $p \in \mathbf{S}$ is called a *zero point* if

$$v_{\mathbf{S}}(p) = \mathbf{0}$$

If there is a neighborhood $U(p)$ such that p is the unique zero in $U(p)$, then p is an *isolated zero point*.

We use

$$\text{Zero}(v_{\mathbf{S}})$$

to denote the set of all zero points of a vector field $v_{\mathbf{S}}$

Definition 92 (Index of Zero Point)**.** Given a zero $p \in \text{Zero}(v_{\mathbf{S}})$ of a vector field $v_{\mathbf{S}}$, choose a small disk $B(p, \varepsilon)$ and define a map φ from ∂B to unit circle $\mathbb{S}^1$:

$$\varphi : \partial B \to \mathbb{S}^1$$

where a point $q \in \partial B$ maps to $\varphi(q) \in \mathbb{S}^1$ with the same vector direction $\dfrac{v_{\mathbf{S}}(q)}{|v_{\mathbf{S}}(q)|}$, which induces a homomorphism:

$$\varphi_{\#} : \pi_1(\partial B) \to \pi_1(\mathbb{S}^1)$$

and must have the form

$$\varphi_{\#}(z) = kz$$

where k is called the *index of zero point*, denoted as

$$k =: \text{Ind}(v_{\mathbf{S}}, p)$$

comment: very similar to "degree of map" and "index of fixed point"

Example 93 (Index of Zero Point)**.** see figure 3.12, if the mapping is with same orientation then we count positive, otherwise count negative. Index of zero point of sink field, source field and saddle field is $+1, +1$ and -1, respectively

Definition 94 (Poincaré-Hopf Index Theorem)**.** Assume $\mathbf{S}$ is a compact, oriented smooth surface, $v_{\mathbf{S}}$ is a smooth tangent vector field with isolated zeros. If $\mathbf{S}$ has boundaries[6], then $v_{\mathbf{S}}$ point along the exterior normal direction[7], then we have

$$\sum_{p \in \text{Zero}(v_{\mathbf{S}})} \text{Ind}(v_{\mathbf{S}}, p) = \chi(\mathbf{S})$$

where $\chi(\mathbf{S})$ is the Euler-Poincaré characteristic.

[6] for a surface $\mathbf{S}$ with genus g and number of boundaries b, the Euler-Poincaré characteristic is

$$\chi(\mathbf{S}) = 2(1 - g) - b$$

[7] for a point $p \in \partial\mathbf{S}$, $v_{\mathbf{S}}(p) \cdot \mathbf{n}(p) > 0$

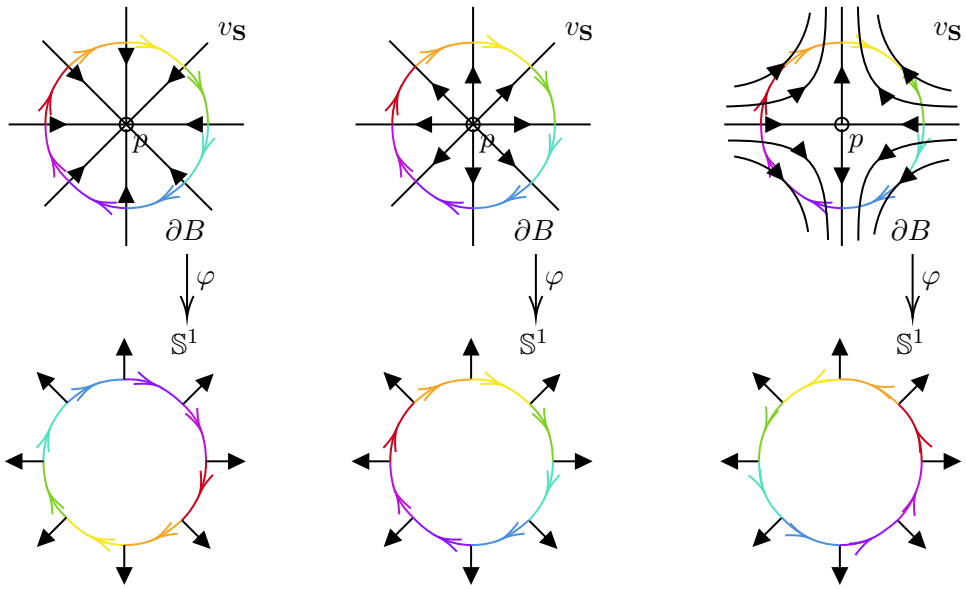

$\mathrm{Ind}(v_{\mathbf{S}}, p) = +1$ $\mathrm{Ind}(v_{\mathbf{S}}, p) = +1$ $\mathrm{Ind}(v_{\mathbf{S}}, p) = -1$

Figure 3.12: index of sink (left), source (middle) and saddle (right) point is $+1, +1, -1$, respectively

Proof. we construct a continuous self-map $f_\varepsilon : \mathbf{S} \to \mathbf{S}$ in following way:

$$f_\varepsilon(p) = p + \varepsilon v_{\mathbf{S}}(p)$$

we know the identity map (where $\varepsilon = 0$) is homotopic to f_ε:

$$f_0 \sim f_\varepsilon$$

thus we have (see example 90)

$$\Lambda(f_\varepsilon) = \Lambda(\mathrm{id}) = \chi(\mathbf{S})$$

notice that

$$f_\varepsilon(p) = p \qquad \text{if and only if} \qquad v_{\mathbf{S}} = \mathbf{0}$$

thus $\Lambda(f_\varepsilon)$, the summation of indices of fixed points of f_ε, equals to the summation of indices of zero points of $v_{\mathbf{S}}$, equals to Euler-Poincaré characteristic

$$\sum_{p \in \mathrm{Fix}(f_\varepsilon)} \mathrm{Ind}(f_\varepsilon, p) = \sum_{p \in \mathrm{Zero}(v_{\mathbf{S}})} \mathrm{Ind}(v_{\mathbf{S}}, p) = \chi(\mathbf{S})$$

□

Example 95 (Poincaré-Hopf Index Theorem)**.** For a torus with $\chi(\mathbf{T}^2) = 0$, one can construct a tangent vector field without zero point. For a sphere with $\chi(\mathbb{S}^2) = 2$ and a bi-torus $\chi(\mathbf{T}^2 \oplus \mathbf{T}^2) = -2$, however, one cannot construct a tangent vector field without zero point. As shown in figure 3.13

Example 96 ("Parietal Whorl" theorem)**.** We now show that parietal whorl in your head is guaranteed by Poincaré-Hopf index theorem.

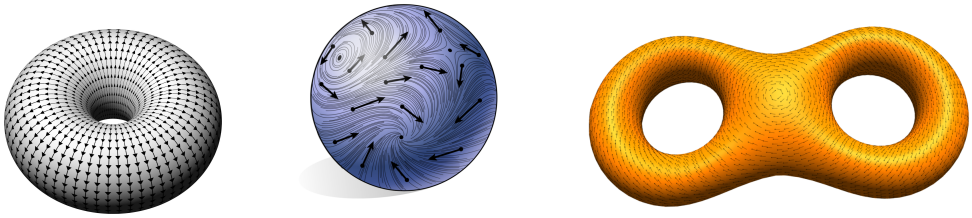

Figure 3.13: tangent vector field of torus, sphere and bi-torus

- The hair region of human scalp can be considered as a smooth, compact, oriented surface with a boundary, so its Euler-Poincaré characteristic is 1
- The hair, with its direction and length, can be considered as a tangent vector field
- The parietal whorl, can be considered the zero point of the vector field

Given the fact that, the hairs on boundary always point along the exterior normal direction, as shown in figure 3.14 for currently-unknown developmental biological reason, Poincaré-Hopf index theorem guarantees that everyone has at least one parietal whorl

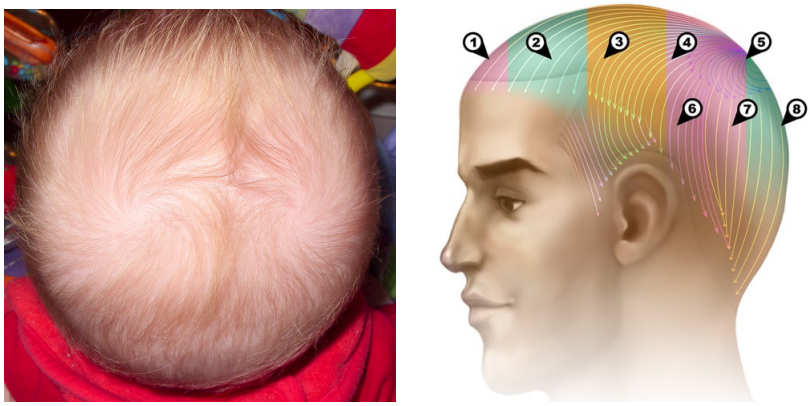

Figure 3.14: A baby with possibly two source points and one saddle point on his head at the same time (left). Hairs on boundary of hair region on your scalp always point outward (right)

Chapter 4

Topological Obstruction

Poincaré-Hopf index theorem tells us that one cannot construct a smooth vector field over a sphere without zero point. Today we see this conclusion from another view.

4.1 Tangent Vector in Coordinate Chart

Historically, geometric techniques were developed mostly for Euclidean space. To study curved space, e.g. a manifold, we can construct local maps of open covers between manifold and Euclidean space.

Definition 97 (Smooth Manifold with Charts and Atlas)**.** A manifold is a topological space $\mathbf{M}$ covered by a set of open sets $\{U_\alpha\}$. A homeomorphism $\varphi_\alpha : U_\alpha \to \mathbb{R}^n$ maps U_α to the Euclidean space $\mathbb{R}^n$. $(U_\alpha, \varphi_\alpha)$ is called a coordinate *chart* of $\mathbf{M}$. The set of all charts $\{(U_\alpha, \varphi_\alpha)\}$ form the *atlas* of $\mathbf{M}$. Suppose $U_\alpha \cap U_\beta \neq \emptyset$, then

$$\varphi_{\alpha\beta} = \varphi_\beta \circ \varphi_\alpha^{-1} : \varphi_\alpha(U_\alpha \cap U_\beta) \to \varphi_\beta(U_\alpha \cap U_\beta)$$

is a *transition map*. If all transition maps are smooth, namely

$$\varphi_{\alpha\beta} \in C^\infty(\mathbb{R}^n)$$

then the manifold is a differentiable (or differential) manifold or a *smooth manifold*, as shown in figure 4.1

Example 98 (Stereo-graphic Projection)**.** A manifold can hardly be covered by only one coordinate chart, thus it usually needs to be covered by multiple charts. A basic example is so-called *stereo-graphic projection*.

As shown in figure 4.2, north pole $\alpha = (0, 0, 1)$, south pole $\beta = (0, 0, -1)$, let $p = (x_1, x_2, x_3)$, $\varphi_\alpha(p) = (x, y)$, $\varphi_\alpha(q) = (u, v)$

$$\begin{aligned}
\varphi_\alpha &: (x_1, x_2, x_3) \mapsto (\frac{x_1}{1 - x_3}, \frac{x_2}{1 - x_3}) \\
\varphi_\alpha^{-1} &: (x, y) \mapsto (\frac{2x}{1 + x^2 + y^2}, \frac{2y}{1 + x^2 + y^2}, \frac{-1 + x^2 + y^2}{1 + x^2 + y^2}) \\
\varphi_\beta &: (x_1, x_2, x_3) \mapsto (\frac{x_1}{1 + x_3}, \frac{-x_2}{1 + x_3}) \\
\varphi_\beta^{-1} &: (u, v) \mapsto (\frac{2u}{1 + u^2 + v^2}, \frac{-2v}{1 + u^2 + v^2}, \frac{1 - u^2 - v^2}{1 + u^2 + v^2})
\end{aligned}$$

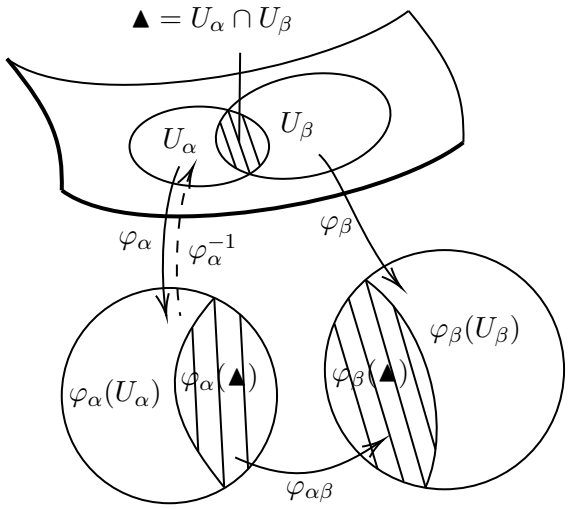

Figure 4.1: definition of smooth manifold was achieved by mapping it to Euclidean space patch by patch smoothly.

Note that indeed $\varphi_{\alpha\beta} = \varphi_\beta \circ \varphi_\alpha^{-1} \in C^\infty$, the unit sphere is a smooth manifold. Notice that φ_α cannot cover α and φ_β cannot cover β. You need both to cover the whole sphere.

As shown in figure 4.3, let $p \in \mathbb{S}^2$. Any vector $d\mathbf{r} \in T_p\mathbb{S}^2$ through φ_α can be represented by $d\mathbf{r} = \partial_x dx + \partial_y dy$, where

$$\partial_x = \frac{\partial \mathbf{r}}{\partial x} = \frac{\partial \varphi_\alpha^{-1}(x,y)}{\partial x} = \frac{2}{(1+x^2+y^2)^2} \begin{bmatrix} 1-x^2+y^2 \\ -2xy \\ 2x \end{bmatrix}$$

$$\partial_y = \frac{\partial \mathbf{r}}{\partial y} = \frac{\partial \varphi_\alpha^{-1}(x,y)}{\partial y} = \frac{2}{(1+x^2+y^2)^2} \begin{bmatrix} -2xy \\ 1+x^2-y^2 \\ 2y \end{bmatrix}$$

and the inner product

$$\langle \partial_x, \partial_x \rangle = \langle \partial_y, \partial_y \rangle = \frac{4}{(1+x^2+y^2)^2}$$

$$\langle \partial_x, \partial_y \rangle = 0$$

so interestingly the bases of $T_p\mathbb{S}^2$ derived from partial derivative are orthogonal with equal length.

Definition 99 (Riemannian Metric and Riemannian Manifold)**.** Let $\mathbf{M}$ be a smooth manifold, a *Riemannian metric* g on $\mathbf{M}$ is a smooth family of inner products on the tangent spaces of $\mathbf{M}$. Namely, g associates to each point $p \in \mathbf{M}$ a positive definite symmetric bi-linear form on $T_p\mathbf{M}$:

$$g_p : T_p\mathbf{M} \times T_p\mathbf{M} \to \mathbb{R}$$

along with which comes a norm

$$|\cdot|_{g_p} : T_p\mathbf{M} \to \mathbb{R} \qquad \text{defined by} \qquad |\mathbf{v}|_{g_p} = \sqrt{g_p(\mathbf{v},\mathbf{v})}$$

The smooth manifold $\mathbf{M}$ endowed with this metric g is a *Riemannian manifold*, denoted by $(\mathbf{M}, g)$. Every smooth manifold has a Riemannian metric.

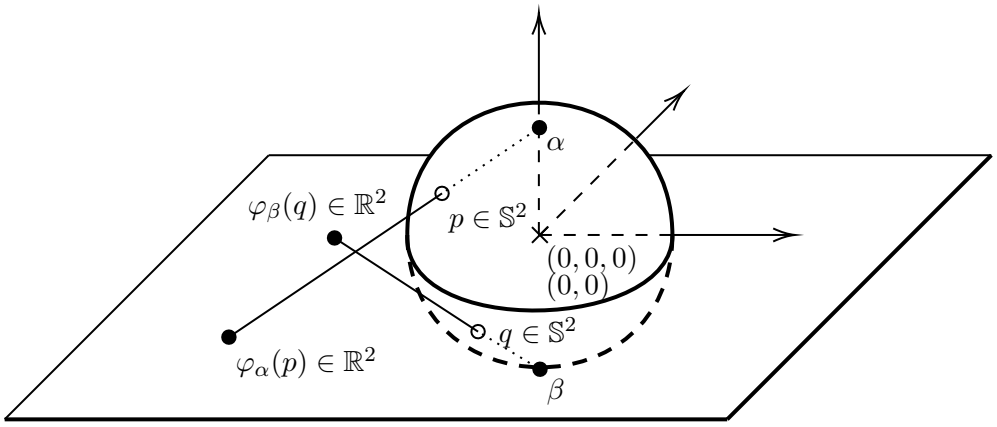

Figure 4.2: A unit sphere $\mathbb{S}^2 \in \mathbb{R}^3$ cannot be covered by only one chart, but can be covered by two charts, so-called stereo-graphic projection. The center of the sphere is $(0,0,0)$. We take its xy-plane as the image plane, containing the equator of sphere. The north pole α projects a point $p \in \mathbb{S}^2$ to the plane $\varphi_\alpha(p) \in \mathbb{R}^2$, and the south pole β projects a point $q \in \mathbb{S}^2$ to the plane $\varphi_\beta(q) \in \mathbb{R}^2$.

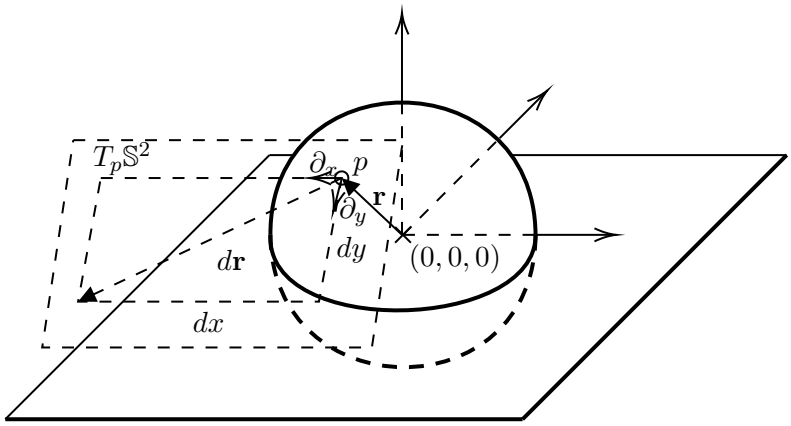

Figure 4.3: Let $p \in \mathbb{S}^2$. Let vector $\mathbf{r} = \varphi_\alpha^{-1}(x,y)$ parametrized by $(x,y) \in \mathbb{R}^2$, then any vector $d\mathbf{r}$ on $T_p\mathbb{S}^2$, the tangent plane at point p on $\mathbb{S}^2$, can be represented by $d\mathbf{r} = \partial_x dx + \partial_y dy$.

Continue example 98. All the coordinates are in $\mathbb{R}^3$. For any tangent vector $d\mathbf{r} = \partial_x dx + \partial_y dy \in T_p\mathbb{S}^2$ at point p, we need (x,y) to parameterize the position of point $p \in \mathbb{S}^2$ and (dx, dy) to parameterize the direction and length of tangent vector $d\mathbf{r}$. We can use (x, y, dx, dy) to parameterize tangent vector.

We now introduce g_p^{can}, the *canonical Euclidean metric*, as a case of Riemannian metric[1] to measure the "distance" of two tangent vector at point p

$g_p^{\text{can}} : T_p\mathbb{S}^2 \times T_p\mathbb{S}^2 \to \mathbb{R}$ is defined by $(\partial_x dx_1 + \partial_y dy_1, \partial_x dx_2 + \partial_y dy_2) \mapsto dx_1 dx_2 + dy_1 dy_2$

if we are only interested in unit tangent vector ("unit" in the sense of g_p^{can}) and denote

[1] Let $x^1, ..., x^n$ denote the standard coordinates on $\mathbb{R}^n$. Then define $g_p^{\text{can}} : T_p\mathbb{R}^n \times T_p\mathbb{R}^n \to \mathbb{R}$ by

$$\left(\sum_i a_i \frac{\partial}{\partial x^i}, \sum_j b_j \frac{\partial}{\partial x^j} \right) \mapsto \sum_i a_i b_i$$

$UT_p\mathbb{S}^2$ as unit tangent space, then we only need

$$|d\mathbf{r}|_{g_p^{\text{can}}} = \sqrt{g_p(d\mathbf{r}, d\mathbf{r})} = \sqrt{(dx)^2 + (dy)^2} = 1$$

then we can re-parameterize (dx, dy) as $(\cos\tau, \sin\tau)$, reducing four parameters to three:

$$(x, y, \tau)$$

if we are further only interested in unit tangent vector on equator of unit sphere, we can re-parameterize (x, y) as $(\cos\theta, \sin\theta)$, reducing three parameters to two:

$$(\theta, \tau)$$

4.2 Shape of Smooth Non-zero Tangent Vector Field

We now consider a Riemann surface $(\mathbf{M}, g)$ with non-zero unit tangent vector everywhere ("unit" is in the sense of g). All the possible unit tangent vector fields, which of course is non-zero, form a unit tangent bundle, denoted by $UT\mathbf{M}$:

$$UT\mathbf{M} := \bigcup_{p\in\mathbf{M}} \{p\}\times UT_p\mathbf{M} = \bigcup_{p\in\mathbf{M}} \{(p, d\mathbf{r}) \mid d\mathbf{r} \in T_p\mathbf{M}, |d\mathbf{r}|_g = 1\} = \{(p, d\mathbf{r}) \mid p \in \mathbf{M}, d\mathbf{r} \in T_p\mathbf{M}, |d\mathbf{r}|_g = 1\}$$

The unit tangent bundle of a surface is a 3-dimensional manifold. Then we consider a Riemann surface of simplest kind: a unit sphere with canonical Euclidean metric $(\mathbb{S}^2, g_p^{\text{can}})$:

$$UT\mathbb{S}^2 = \{(p, d\mathbf{r}) \mid p \in \mathbb{S}^2, d\mathbf{r} \in T_p\mathbb{S}^2, |d\mathbf{r}|_{g_p^{\text{can}}} = 1\}$$

Poincaré-Hopf theorem tells us that it is **impossible** to construct a **smooth** $v_{\mathbb{S}^2} \in UT\mathbb{S}^2$. We demonstrate such impossibility by topological obstruction.

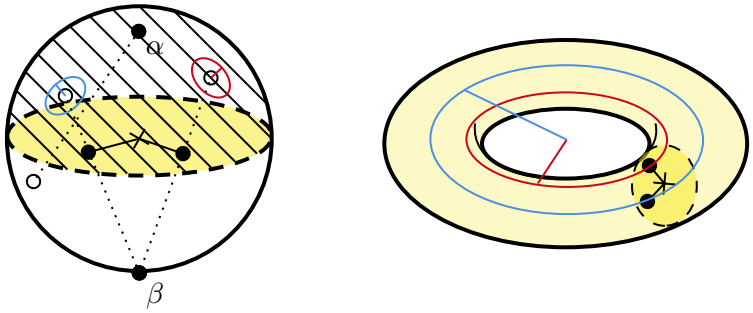

Figure 4.4: The topological space of unit tangent bundle of unit hemisphere is $\mathbb{S}^1 \times \mathbb{D}^2$, a solid torus. The sectioning disk in solid torus (deep yellow) corresponds to the image plane of φ_β, for example

We know that coordinate chart φ_α cannot cover point α and coordinate chart φ_α cannot cover point β. So we use φ_α for lower hemisphere and φ_β for upper hemisphere (figure 4.4), and glue them together through **equator**. We will show that to construct a smooth $v_{\mathbb{D}^2} \in UT\mathbb{D}^2$, the unit tangent vector field over unit hemisphere[2], **is okay**.

[2] we use $\mathbb{D}^2$ to denote a unit disk, which is homotopic to unit hemisphere, so we also use $\mathbb{D}^2$ to denote unit hemisphere

But when we glue them together with constraint of smooth transition from φ_α to φ_β on equator, two hemispheres **cannot allow smooth vector fields over them at the same time**.

Firstly, we see that the shape of $UT\mathbb{D}^2$ is a **solid** torus

$$UT\mathbb{D}^2 \sim \mathbb{S}^1 \times \mathbb{D}^2$$

as shown in figure 4.4. Because $UT_p\mathbb{D}^2$, the set of all possible directions of unit tangent vector at a point on unit hemisphere, corresponds to a **fiber** that goes through a point on sectioning disk in solid torus (e.g. the red and blue curves in figure 4.4)

$$UT_p\mathbb{D}^2 \sim \mathbb{S}^1$$

If we cut the torus (to remove its genus), then the sectioning surface represents a particular $v_{\mathbb{D}^2}$. The sectioning surface, through which every fiber goes only once, is called **global section**. The smoothness of $v_{\mathbb{D}^2}$ is guaranteed by the smoothness of that global section. All the possible smooth $v_{\mathbb{D}^2}$ corresponds to all the possible global sections that can be smoothly deformed from the sectioning disk in solid torus

$$v_{\mathbb{D}^2} \sim \mathbb{D}^2$$

Secondly, notice that $UT(\partial\mathbb{D}^2)$, the unit tangent bundle of unit hemisphere on equator (the boundary of hemisphere) corresponds to a torus, the surface of that solid torus (figure 4.4)

$$UT(\partial\mathbb{D}^2) = UT\mathbb{S}^1 = \partial(\mathbb{S}^1 \times \mathbb{D}^2) = \mathbb{S}^1 \times (\partial\mathbb{D}^2) = \mathbb{S}^1 \times \mathbb{S}^1 = \mathbf{T}^2$$

thus gluing two smooth $v_{\mathbb{D}^2}$ on equator smoothly, let's say $v_{\mathbb{D}^2_L}$ ("L" for lower hemisphere) and $v_{\mathbb{D}^2_U}$ ("U" for upper hemisphere), is very much of gluing two solid tori with homeomorphism of two tori such that two global sections, let's say $\mathbb{D}^2_L$ and $\mathbb{D}^2_U$, forming a larger global section of $UT(\mathbb{S}^2)$

$$v_{\mathbb{D}^2_L} \bigcup_{UT(\partial\mathbb{D}^2_L)\sim UT(\partial\mathbb{D}^2_U)} v_{\mathbb{D}^2_U} \sim \mathbb{D}^2_L \bigcup_{\mathbf{T}^2_L\sim\mathbf{T}^2_U} \mathbb{D}^2_U$$

The topological obstruction means that one cannot find a global section of $UT(\mathbb{S}^2)$. Or in other words, with constraint of $\mathbf{T}^2_L \sim \mathbf{T}^2_U$, by setting a global section $\mathbb{D}^2_L$ of lower solid torus freely, one cannot find a global section of upper solid torus, as we show later.

4.3 Topological Obstruction

The homeomorphism of two tori was guaranteed by smooth transition of charts on equator from φ_α to φ_β, namely, from (x, y, dx, dy) to (u, v, du, dv). We check how different φ_β from φ_α, continue example 98

$$\partial_u = \frac{\partial \mathbf{r}}{\partial u} = \frac{\partial \varphi_\beta^{-1}(u,v)}{\partial u} = \frac{2}{(1+u^2+v^2)^2} \begin{bmatrix} 1-u^2+v^2 \\ 2uv \\ -2u \end{bmatrix}$$

$$\partial_v = \frac{\partial \mathbf{r}}{\partial v} = \frac{\partial \varphi_\beta^{-1}(u,v)}{\partial v} = \frac{2}{(1+u^2+v^2)^2} \begin{bmatrix} -2uv \\ -1-u^2+v^2 \\ -2v \end{bmatrix}$$

$$\langle \partial_u, \partial_u \rangle = \langle \partial_v, \partial_v \rangle = \frac{4}{(1+u^2+v^2)^2}$$
$$\langle \partial_u, \partial_v \rangle = 0$$

smooth transition from (dx, dy) to (du, dv) is guaranteed by differentiable Jacobian $\begin{bmatrix} u_x & u_y \\ v_x & v_y \end{bmatrix}$:

$$\begin{bmatrix} du \\ dv \end{bmatrix} = \begin{bmatrix} u_x & u_y \\ v_x & v_y \end{bmatrix} \begin{bmatrix} dx \\ dy \end{bmatrix}$$

To compute $u_x = \dfrac{\partial u}{\partial x}, u_y = \dfrac{\partial u}{\partial y}, v_x = \dfrac{\partial v}{\partial x}$ and $v_y = \dfrac{\partial v}{\partial y}$, the most convenient way is by complex variable. If we parameterize (x, y) by complex number $z = x + iy$ and (u, v) by $w = u = iv$, notice that

$$\frac{1}{z} = \frac{1}{x+iy} = \frac{x-iy}{x^2+y^2} = \frac{\left(\dfrac{x_1}{1-x_3}\right) - i\left(\dfrac{x_2}{1-x_3}\right)}{\left(\dfrac{x_1}{1-x_3}\right)^2 + \left(\dfrac{x_2}{1-x_3}\right)^2} = \frac{x_1(1-x_3) - ix_2(1-x_3)}{\underbrace{(x_1^2+x_2^2+x_3^2)}_{1} - x_3^2} = \frac{x_1 - ix_2}{1+x_3} = u + iv = w$$

with $\dfrac{1}{z} = w$, we have $dw = -\dfrac{1}{z^2}dz$, we write

$$du + idv = -\frac{1}{z^2}(dx + idy) = -\frac{1}{(x+iy)^2}(dx + idy) = \frac{1}{(x^2+y^2)^2} \begin{bmatrix} dx(y^2-x^2) - dy(2xy) & \hookleftarrow \\ +i[dy(y^2-x^2) + dx(2xy)] \end{bmatrix}$$

then by technique of complex variable:

$$\begin{bmatrix} u_x & u_y \\ v_x & v_y \end{bmatrix} = \frac{1}{(x^2+y^2)^2} \begin{bmatrix} y^2-x^2 & -2xy \\ 2xy & y^2-x^2 \end{bmatrix}$$

is indeed differentiable near by $x^2 + y^2 = 1$, the equator.

Moreover, the transition of charts $\varphi : (z, dz) \mapsto (w, dw)$ is

$$\varphi : (z, dz) \mapsto (\frac{1}{z}, -\frac{1}{z^2}dz)$$

On equator, if parametrized by (θ, τ), as $z = e^{i\theta}$ and $dz = e^{i\tau}$, we have

$$\varphi : (\theta, \tau) \mapsto (-\theta, \pi - 2\theta + \tau)$$

We use canonical representation of $\pi_1(\mathbf{T}_L^2)$ and $\pi_1(\mathbf{T}_U^2)$:

$$\pi_1(\mathbf{T}_L^2) = \langle a_L, b_L | [a_L, b_L] \rangle$$
$$\pi_1(\mathbf{T}_U^2) = \langle a_U, b_U | [a_U, b_U] \rangle$$

then φ induces a push-forward map on homotopy group[3]:

$$\varphi_\# : \pi_1(\mathbf{T}_L^2) \to \pi_1(\mathbf{T}_U^2)$$

by

$$a_L \mapsto a_U$$
$$b_L \mapsto a_U^{-2} b_U^{-1}$$

As shown in figure 4.5, we finish construction of a topological obstruction to show that one cannot construct a smooth vector field over a sphere without zero point.

[3]check by corner points: e.g. $A = (0,0) \mapsto \varphi(A) = (0,\pi), B = (0,2\pi) \mapsto \varphi(B) = (0,3\pi), C = (2\pi,2\pi) \mapsto \varphi(C) = (-2\pi,-\pi), D = (2\pi,0) \mapsto \varphi(D) = (-2\pi,-3\pi)$

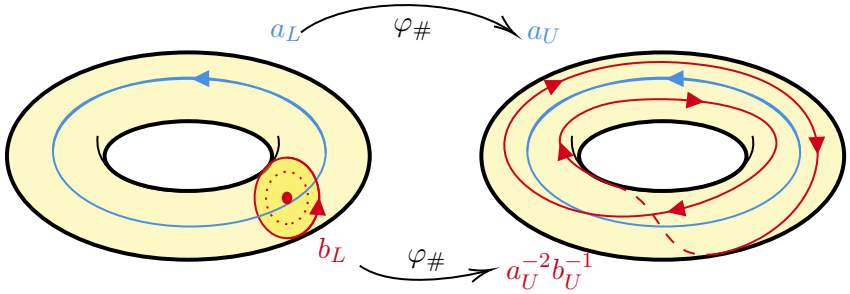

Figure 4.5: With constraint $\mathbf{T}_L^2 \sim \mathbf{T}_U^2$, by setting the global section $\mathbb{D}_L^2$ freely in lower solid torus, its boundary $\partial\mathbb{D}_L^2 = b_L$ maps to $a_U^{-2}b_U^{-1}$. While b_L can shrink to a point, $a_U^{-2}b_U^{-1}$ cannot, thus one cannot find a global section in upper solid torus with $a_U^{-2}b_U^{-1}$ as its boundary, which leads to a topological obstruction

4.4 Shape of Unit Tangent Bundle of Unit Sphere

We can derive the fundamental group of $UT\mathbb{S}^2$ using Van Kampen theorem.

Theorem 100 (Van Kampen (-Seifert) Theorem)**.** *Topological space* $\boldsymbol{M}$ *is decomposed into the union of* $\mathbf{U}$ *and* $\mathbf{V}$*, the intersection of* $\mathbf{U}$ *and* $\mathbf{V}$ *is* $\boldsymbol{W}$*,*

$$\boldsymbol{M} = \boldsymbol{U} \cup \boldsymbol{V}$$

$$\boldsymbol{W} = \boldsymbol{U} \cap \boldsymbol{V}$$

where $\mathbf{U}$*,* $\mathbf{V}$ *and* $\boldsymbol{W}$ *are path connected.*

$$i : \boldsymbol{W} \hookrightarrow \mathbf{U}$$

$$j : \boldsymbol{W} \hookrightarrow \mathbf{V}$$

are the inclusion maps. Pick a base point $p \in \boldsymbol{W}$*, the fundamental groups*

$$\pi_1(\mathbf{U}, p) = \langle u_1, ..., u_k | \alpha_1, ..., \alpha_l \rangle$$

$$\pi_1(\mathbf{V}, p) = \langle v_1, ..., v_m | \beta_1, ..., \beta_n \rangle$$

$$\pi_1(\mathbf{W}, p) = \langle w_1, ..., w_p | \gamma_1, ..., \gamma_q \rangle$$

then $\pi_1(\mathbf{M}, p)$ *is given by*

$$\pi_1(\mathbf{M}, p) = \langle u_1, ..., u_k, v_1, ..., v_m | \alpha_1, ..., \alpha_l, \beta_1, ..., \beta_n, i(w_1)j(w_1)^{-1}, ..., i(w_p)j(w_p)^{-1} \rangle$$

One can use Van Kampen's theorem to compute fundamental groups for topological spaces that can be decomposed into simpler spaces.

Example 101 (Fundamental Group of Unit Tangent Bundle of Unit Sphere)**.** We glue $UT\mathbb{D}_L^2$ and $UT\mathbb{D}_U^2$ with homomorphism:

$$\varphi_\#(a_L) = a_U$$

$$\varphi_\#(b_L) = a_U^{-2}b_U^{-1}$$

thus the set up:

$$UT\mathbb{S}^2 = UT\mathbb{D}^2_L \bigcup_{\mathbf{T}^2_L \sim \mathbf{T}^2_U} UT\mathbb{D}^2_U$$

$$\mathbf{T}^2 = UT\mathbb{D}^2_L \bigcap UT\mathbb{D}^2_U$$

where $UT\mathbb{D}^2_L$, $UT\mathbb{D}^2_U$ and $\mathbf{T}^2$ are path connected.

$$i : \mathbf{T}^2 \hookrightarrow UT\mathbb{D}^2_L$$

$$j : \mathbf{T}^2 \hookrightarrow UT\mathbb{D}^2_U$$

are the inclusion maps. Pick a base point $p \in \mathbf{T}^2$, the fundamental groups

$$\pi_1(UT\mathbb{D}^2_L, p) = \langle a_L \rangle \qquad \pi_1(\mathbf{T}^2_L, p) = \langle a_L, b_L | [a_L, b_L] \rangle$$

$$\pi_1(UT\mathbb{D}^2_U, p) = \langle a_U \rangle \qquad \pi_1(\mathbf{T}^2_U, p) = \langle a_U, b_U | [a_U, b_U] \rangle$$

$$\pi_1(\mathbf{T}^2, p) = \langle a, b | [a, b] \rangle$$

the inclusion maps

$$i(a) = a_L, j(a) = a_U^{-1}$$

$$i(b) = b_L = \emptyset, j(b) = (a_U^{-2} b_U^{-1})^{-1}$$

then $\pi_1(UT\mathbb{S}^2, p)$ is given by

$$\pi_1(UT\mathbb{S}^2, p) = \langle a_L, a_U | a_L a_U, a_U^{-2} b_U^{-1} \rangle \cong \mathbb{Z}_2$$

4.5 Obstruction Class

The information of topological obstruction can be encoded in a 2-form Ω of smooth surface $\mathbf{M}$. The 2-form Ω is computed by random generated smooth vector field over $\mathbf{M}$. Surprisingly, all Ω generated in this way are cohomological to each other, thus they form an equivalence class, which we call it **obstruction class**. We denote $[\Omega]$ as obstruction class of $H^2(\mathbf{M}, \mathbb{R})$.

Definition 102 (Obstruction Class)**.** Let $\mathbf{M}$ be a smooth manifold. According to simplicial approximation theorem, there exists $\mathbf{M}_\Delta$, the triangulation of $\mathbf{M}$, which is refined enough up to any precision. Given $\mathbf{M}_\Delta$, we proceed without loss of generality. The unit tangent bundle of every 2-simplex $[v_i, v_j, v_k]$, is direct product of fiber and the 2-simplex:

$$UT[v_i, v_j, v_k] = \mathbb{S}^1 \times [v_i, v_j, v_k]$$

then we generate random tangent vector for each vertex, which means we generate three random points on the torus $UT(\partial[v_i, v_j, v_k])$, the surface (or boundary) of solid torus $UT[v_i, v_j, v_k]$. We see if the loop $\gamma \in UT(\partial[v_i, v_j, v_k])$ that goes through those three points can shrink to a point

Since $\pi_1(UT[v_i, v_j, v_k]) \cong \mathbb{Z}$, should $\gamma \in \pi_1(UT[v_i, v_j, v_k])$ give a number, which we assign it to the 2-form $\Omega([v_i, v_j, v_k])$, either zero if γ can shrink to a point, or non-zero if a local topological obstruction occurs, as shown in figure 4.6. In the end, we will have a 2-form Ω which represents the *obstruction class*

$$[\Omega] \in H^2(\mathbf{M}, \mathbb{R})$$

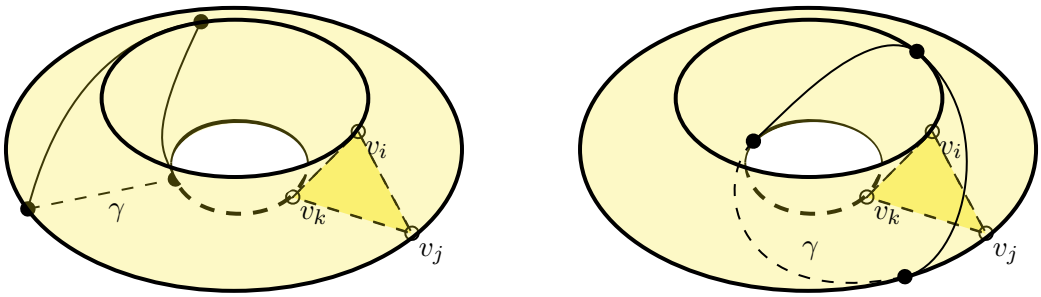

$\Omega(\gamma) \leftarrow 0$ $\Omega(\gamma) \leftarrow a \neq 0$

Figure 4.6: illustration of local topological obstruction

HRIPIE Member

Summer 2020

徐雪阳 中山大学电信学院硕士生

苏燮阳 纽约大学计算机工程硕士生

Fall 2020

陈子嘉 波士顿大学计算机科学/统计学本科生

王来友 广东药科大学药学系教授

honzresearch.github.io

Honz
Research
Institute of
Pharmacometrics and
Industrial
Engineering